AN ABSTRACT OF THE THESIS OF

Shyr Tung Luo for the degree of Master of Science in Nuclear Engineering presented on May 11,1982

Title: Development and Implementation of an Improved Formulation of the Momentum Balance for a Once-Through Steam Generator Transient Model

Abstract approved: Redacted for Privacy

K. Hornyik

A detailed formulation of the momentum equation including the Baroczy model for two phase friction is presented in this thesis. Numerical techniques for solving this equation along with the remainder of the describing equations are also presented. This model has been incorporated into an existing thermal hydraulic code for simulating the steady state and transient performance of a Once-Through Steam Generator. A number of representative cases have been studied with this model. Based on this study we note that for accurate steam generator modeling over the range of anticipated operation a complete momentum balance model is required.

DEVELOPMENT AND IMPLEMENTATION OF AN IMPROVED FORMULATION OF THE MOMENTUM BALANCE FOR A ONCE THROUGH STEAM GENERATOR TRANSIENT MODEL

by

Shyr Tung Luo

A THESIS

submitted to

Oregon State University

in partial fulfillment of

the requirements for the

degree of

Master of Science

Completed May 11, 1982

Commencement June, 1983

APPROVED

Redacted for Privacy

Associate Professor of Nuclear Engineering
in charge of major

Redacted for Privacy

Head of Department of Nuclear Engineering

Redacted for Privacy

Dean of Graduate School

Date thesis is presented May 11, 1982

Type by Shyr Tung Luo

ACKNOWLEDGEMENT

I wish to extend my deepest appreciation to Dr. K. Hornyik, my major professor and thesis advisor. His helpful suggestions made completion of this thesis possible. I also gratefully acknowledge the Gesellschaft für Reaktorsicherheit for funding this research.

I would like to dedicate this work to my parents, Wenshih Luo and Tsungfung Wang for their love and patience.

TABLE OF CONTENTS

LIST OF FIGURES

Figure Page

LIST OF TABLES

LIST OF SYMBOLS

B = Baroczy property index, dimensionless

C = constant for friction factor in turbulant flow

Cp = tube metal specific thermal capacity, J/kg

Dh = hydraulic diameter, m

F = force, N

Fg = Baroczy two-phase multiplier ratio, dimensionless

f = friction coefficient, dimensionless

fs = friction coefficient for single-phase flow

ft = friction coefficient for two-phase flow

G = mass velocity, kg/(sec-sq. m)

G1 = mass velocity for primary fluid

G1i= inlet mass velocity of primary fluid

G2 = mass velocity for secondary fluid

G2i= inlet mass velocity of secondary fluid

Gr = reference mass velocity in Baroczy model

g = gravitational constant, m/(sq. sec)

H = heat transfer coefficient, W/(C-sq. m)

h = specific enthalpy, J/kg

h1 = enthalpy for primary fluid

h1i= inlet enthalpy of primary fluid

h2 = enthalpy for secondary fluid

h2i= inlet enthalpy of secondary fluid

i = index of z-axis

j = index of time

K = constant for spacer pressure drop

Kp = constant for pressure drop model in the OLD code

Kt = tube metal thermal conductivity, W/C-m

Mw = wetted perimeter of duct, m

P = pressure, Pa

P1 = pressure of primary fluid

P2 = Pressure of secondary fluid

P1i= inlet pressure of primary fluid

P2i= inlet pressure of secondary fluid

P2o= outlet pressure of secondary fluid

PE = boundary condition for outlet pressure

PI = inlet pressure

Q2 = heat transfer rate into secondary side, W

qw = heat flux into fluid, W/(sq. m)

qw1= heat flux into primary fluid

qw2= heat flux into secondary fluid

R = sum of pressure gradient resulting from fluid acceleration, friction and gravitation, Pa/m

r = radius, m

r1 = inner radius of tube metal

r2 = outer radius of tube metal

Re = Reynolds number, dimensionless

S = total cross section of tube, sq. m

T = temperature, C

Tb = bulk temperature of fluid

Tb1= bulk temperature of primary fluid

Tb2= bulk temperature of secondary fluid

Ts = surface temperture of tube metal

Tt = tube metal temperture

t = time, sec

u = internal energy of fluid, J/kg

V = volume, cu. m

v = velocity, m/sec

W = property of fluid

X = quality of fluid, %

X1 = quality of primary fluid

X2 = quality of secondary fluuid

Z = distance from bottom of tube bundle, m

Δ = designates a difference when used as a prefix

ΔP = total pressure drop

ΔPg= gravitational pressure drop

ΔPs= spacer pressure drop

ΔPf= friction pressure drop

ΔPa= acceleration pressure drop

ΔPt= transient acceleration pressure drop

μ = viscosity

μ_1 = viscosity for saturated liquid

μ_v = viscosity for saturated vapor

ρ = density, kg/(cu. m)

$\rho 1$ = density of primary fluid

$\rho 2$ = density of secondary fluid

ρt = density of tube metal

ρ_l = density of saturated liquid

ρ_v = density of saturated vapor

τ = shear stress, kg/(sec-sq. m)

ϕ^2 = Baroczy two-phase multiplier

ϕ_r^2 = Baroczy two-phase multiplier for G=Gr

DEVELOPMENT AND IMPLEMENTATION OF AN IMPROVED FORMULATION OF THE MOMENTUM BALANCE FOR A ONCE THROUGH STEAM GENERATOR TRANSIENT MODEL

1. INTRODUCTION

Beside the reactor itself, the steam generator is one of the principal components in a pressurized water reactor (PWR). The steam generator transfers the heat from the primary loop to the secondary loop as shown in Figure 1-1. Heat is generated by fission in the reactor core. It is convected from there by the primary coolant and passed on to the secondary loop by way of the steam generator. Eventually heat is transformed to electric power by the turbine-generator. As shown in this simple scheme the steam generator therefore is the coupling link between the primary and the secondary loop in the PWR plant. This indicates that it is essential to have a good understanding of the steady-state and transient behavior of the steam

generator for predicting PWR response under normal and accidental conditions. This work modifies an earlier version of a code for describing Once-Through Steam Generator (OTSG) steady state and transient behavior[1-5].

The old code (OLD) uses an input pressure profile to define the steam generator fluid condition in the steady state. Based on the assumption that pressure drops are due to friction only and using a simplified friction model, pressure loss coefficients are calculated from this steady state profile. These coefficients are used to then describe the pressure distribution under transient condition. The modified code (NEW) uses a more rigorous formulation of the law of momentum conservation, including the effects of inertial, gravitational and friction forces. The latter are formulated in terms of the empirical Baroczy model which accounts for two-phase effects. It can be expected that this new model will yield a more accurate response and may be applied over a wider range of conditions.

A more recent design of the OTSG is the Integral Economizer OTSG (IEOTSG). As of this date no plant using this design has been put into operation although there are several under construction. This work is intended specifically to model this design and thus provide a tool for performing safety analysis for the purpose of plant licensing. With this improved pressure drop model, the NEW code

will yield more accurate results for a wider range of transients. The NEW code will be integrated into the PWR system code, ALMOD, so that responses involving the entire plant can be simulated.

Chapter 2 reviews the basic model used in the OLD version of the steam generator description, including the basic assumptions, conservation equations and state equations. Two-phase conditions are described in terms of the homogeneous equilibrium model. In chapter 3, the modified model for pressure drop calculation is presented, together with a numerical iteration scheme for solving the pressure boundary condition problem. In chapter 4, we present a detailed investigation of the Baroczy model employed to describe two-phase friction effects. Finally, in chapter 5, we discuss the results of the NEW code for some reference cases.

1. Reactor
2. Core
3. Primary coolant
4. Steam Generator
5. Steam line
6. Turbine
7. Condenser
8. Feed water pump
9. Secondary Condensate line
10. Primary coolant pump

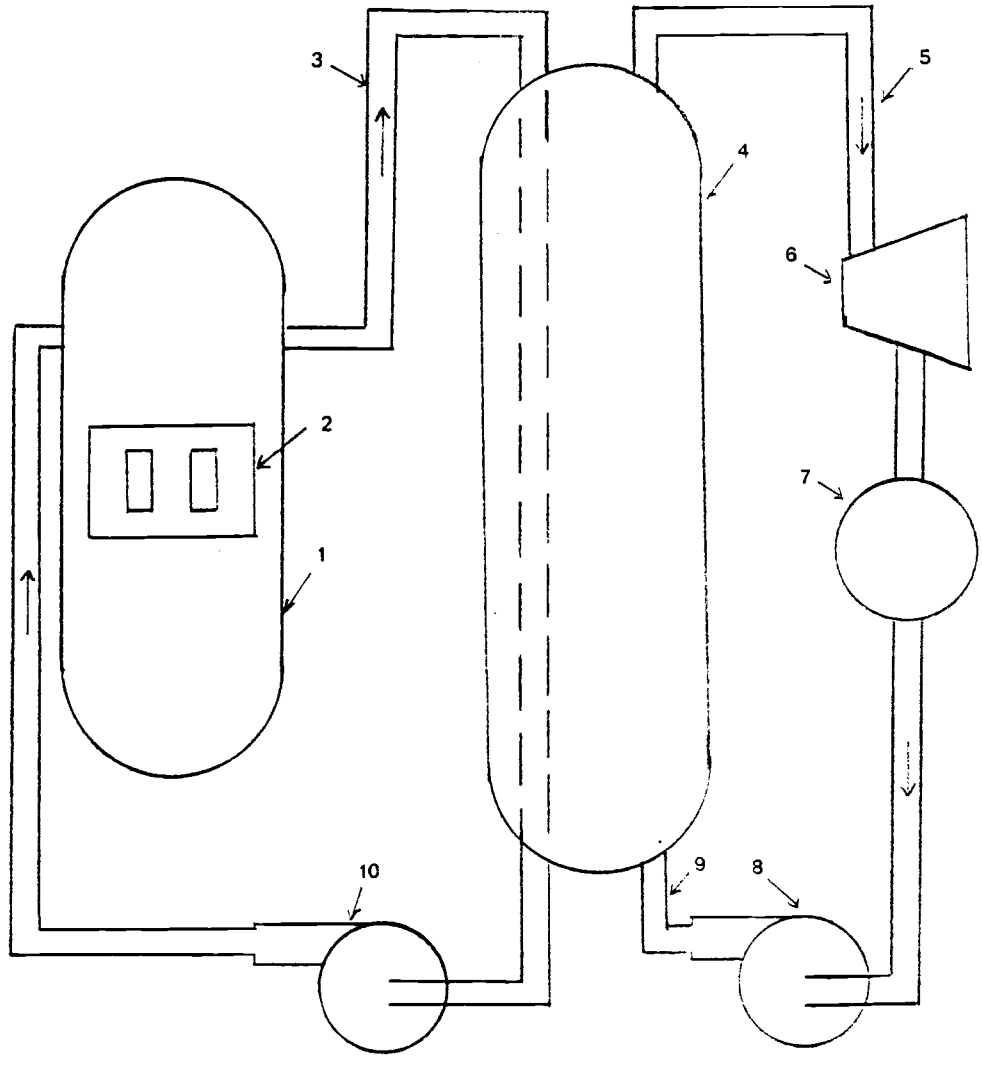

Figure 1-1 Simplified PWR Schematic

2. BACKGROUND

2.1. Channel Flow Model Assumptions

The IEOTSG described in Appendix A can be characterized as a vertical, tube-and-shell heat exchanger with a boiling secondary fluid flow and a subcooled primary flow. The steam generator can thus be represented by channel flow equations describing primary and secondary sides, coupled by the equations for heat transfer through the tube walls.

The fluid dynamic nature of the secondary fluid varies from a nearly incompressible liquid in the inlet region to a highly compressible vapor in the superheated region. Among others, the effect of thermal expansion due to the heating is important to the dynamic behavior. In view of the observed characteristics, a one-dimensional, homogeneous equilibrium model was selected as it appears appropriate for modeling the fluid flow conditions in the OLD code. The principal assumptions made to simplify the modeling of steam generators are:

(1) one-dimensional flow, assuming uniform properties over the flow channel cross sectional area for both primary and secondary fluids

(2) single-channel flow model for both primary and

secondary fluids

(3) single-fluid homogeneous equilibrium model for two-phase flow

(4) incompressible fluid on the primary side

(5) neglect of kinetic energy and potential energy in the fluid energy equations, and

(6) neglect of axial heat conduction both in fluid and the tube wall.

Assumption 1 is considered reasonable for the modeling of steam generator dynamic behavior in view of the large ratio of channel flow length to channel width. In the case of once-through steam generators, tests have been performed using small bundle steam generators with full scale channel geometry[1]. The results of these tests indicate that the steam generator performance is nearly independent of bundle size. The geometry of the channel is characterized by the hydraulic diameter (Dh) which is defined by

$$Dh = 4*S/Mw$$

where S is the total cross section of the stream and Mw is the wetted perimeter of the duct. The hydraulic diameter concept is used for computing the heat-transfer coefficients and pressure drops of the primary as well as the secondary side. An approximation used for describing

two-phase flow conditions is the homogeneous equilibrium model[6], in which both phases, liquid and vapor are assumed to be homogeneously mixed and are moving with the same velocity. Also, thermodynamic equilibrium is assumed between the two phases (i.e., equal temperature and pressure). Assumption 4 is reasonable when we recognize that the primary loop is subcooled liquid under conditions considered here. The energy terms omitted under assumption 5 are known to be negligibly small compared to convective energy contributions in steam generators. Likewise, axial heat conduction can be neglected compared to radial heat conduction and fluid convective heat transfer for conditions existing in steam generators.

2.2. The Governing Equations of Channel Flow

The general partial differential equations which describe mass, momentum and energy conservation for Eulerian single fluid flow are found in the literature (e.g. References (7) and (8)). In applying these equations to our steam generator model we will make use of the assumptions stated above. Thus the partial differential equations are reduced to a one-dimensional form in terms of the flow direction-Z. The resulting conservation equations (see Appendix B) for fluid mass, momentum and energy, respectively, are written as

$$\frac{\partial \rho}{\partial t} = - \frac{\partial G}{\partial z} \qquad (2\text{-}1)$$

$$\frac{\partial G}{\partial t} = - \frac{\partial P}{\partial z} + R \qquad (2\text{-}2)$$

$$\frac{\partial}{\partial t}(\rho * h) = - \frac{\partial}{\partial z}(G * h) + 4 * qw/Dh + \frac{\partial P}{\partial t} \qquad (2\text{-}3)$$

where ρ = fluid density

P = pressure

h = specific enthalpy

qw= wall heat flux into fluid

G = mass velocity or mass flow rate per unit cross section

R = the sum of fluid pressure gradient terms resulting from fluid acceleration, wall friction and gravitational force

In the case of the single-fluid homogeneous equilibrium model for two-phase flow the mass velocity G is given as

$$G = \rho * v$$

where v is the fluid velocity.

The OLD code use a simplified version of equation 2-2, which is obtained by omitting the term on the left hand side, and by defining the term R on the right hand side as

$$R = Kp*G**2/\rho$$

which is recognized as the classic representation of friction loss effects. The value of the constant Kp is determined by prescribing a pressure profile at time t=0, and then is used for the subsequent transient analysis.

An equation of state is required to complete the description of the fluid. The equation of state for water is obtained by interpolation of steam tables, formally represented by the relation:

$$\rho = \rho(P,h) \qquad (2\text{-}4)$$

$$Tb = Tb(P,h) \qquad (2\text{-}5)$$

where Tb is the bulk fluid temperature.

Both primary and secondary side fluid flows can be represented by use of equations 2-1 through 2-5. The heat flux through the tube can be described by use of the heat conduction equation in cylindrical geometry as applies to the solid tube metal[9]

$$\rho_t * Cp * \frac{\partial Tt}{\partial t} = \frac{1}{r} * \frac{\partial}{\partial r}\left(Kt * r * \frac{\partial Tt}{\partial r}\right) \qquad (2\text{-}6)$$

Fluid conditions and tube wall surface conditions are coupled by Newton's law of cooling[9]

$$qw = H*(Tb-Ts) \qquad (2\text{-}7)$$

which is applied for heat transfer at the fluid-tube wall interface for both primary and secondary fluids. In the above equations we used the following quantities:

ρ_t = tube metal density
Ts = tube metal surface temperature
Kt = tube metal thermal conductivity
Cp = tube metal specific thermal capacity
Tt = tube metal temperature, function of r and Z
H = heat transfer coefficient for the solid fluid interface

The tube metal properties Kt, Cp and ρ_t in equation 2-6 are assumed to be constants. The heat transfer coefficient H in equation 2-7 is determined by empirical correlations as a function of fluid flow conditions and tube wall

temperature.

The fluid flow and heat transfer model represented by equations 2-1 through 2-5 includes six dependent variables P, ρ, h, G, qw and Tb. By coupling the heat conduction solution for qw and Ts we may solve equations 2-1 through 2-5 for ρ, P, h, G and Tb for a single-phase fluid. Since a homogeneous model is used which assumes a uniform velocity for two-phase flow, both the primary and secondary sides can be represented by the same equations.

2.3. Boundary Conditions

In section 2.2 we introduced five equations for each side (i.e., primary and secondary side) and three coupling equations thus obtaining a total of 13 equations for 13 unknowns P1, P2, ρ1, ρ2, h1, h2, G1, G2, qw1, qw2, Tb1, Tb2 and Tt. Indices 1, 2 and t represent quantities pertaining to the primary side, the secondary side and the tube wall, respectively. Among these equations we have 7 partial differential equations. One of them is of the second order and the others are of the first order. Therefore, we need 8 boundary conditions. Two of these boundary conditions are interface conditions between the tube and fluid. They are

$$qw1 = + Kt * \frac{\partial Tt}{\partial r}\bigg|_{r=r1} \qquad (2\text{-}8)$$

$$qw2 = - Kt * \left.\frac{\partial Tt}{\partial r}\right|_{r=r2} \qquad (2\text{-}9)$$

where r1 and r2 is the inner and outer radius of the tube.

The other six boundary conditions can be chosen arbitrarily from the inlet or outlet conditions of the fluid. The choices made for the OLD code are

P1i, G1i, h1i

P2o, G2i, h2i

where letter i and o represent inlet and outlet conditions, respectively. Selecting P2o as the boundary condition rather than P2i was done in view of future expansion of the model to include a more detailed description of the steam lines. Instead of using enthalpy as boundary condition, temperature can be used for single phase fluid (liquid or vapor) and quality can be used for two-phase fluid. The equations prescribed above along with the boundary conditions are expected to provide a complete description of the thermal-hydraulic processes in the steam generator. By application of suitable numerical techniques we therefore expect to obtain unique solutions over as wide a range of boundary conditions as may be of practical interest.

3. PRESSURE DROP MODEL

3.1. Momentum Equation

The momentum equation (i.e., equation 2-2) was derived in Appendix B. The parameter R in the momentum equation given by equation 2-2 represents the sum of fluid pressure gradient terms resulting from fluid acceleration, wall friction and gravitational force, that is

$$R = \left(\frac{\partial P}{\partial z}\right)_{acc} + \left(\frac{\partial P}{\partial z}\right)_{frict} + \left(\frac{\partial P}{\partial z}\right)_{grav} \qquad (3\text{-}1)$$

The individual pressure gradient terms in the case of single-phase or homogeneous two-phase flow are determined by

$$\left(\frac{\partial P}{\partial z}\right)_{acc} = -\frac{\partial}{\partial z}(\rho^* v^2) = -\frac{\partial}{\partial z}\left(\frac{G^2}{\rho}\right) \qquad (3\text{-}2)$$

$$\left(\frac{\partial P}{\partial z}\right)_{frict} = -\frac{2f}{Dh} * (\rho^* v^2) = -\frac{2fG^2}{\rho Dh} \qquad (3\text{-}3)$$

$$\left(\frac{\partial P}{\partial z}\right)_{grav} = -\rho^* g \qquad (3\text{-}4)$$

where

f = friction coefficient which is obtained from empirical data as will be discussed in

chapter 4

g = gravitational acceleration in the negative Z-direction.

3.2. Finite Difference Representation of the Momentum Equation

The pressure drop of the steam generator is characterized by significant variation of fluid properties along the heated flow paths. In order to perform integration of the partial differential equations we have chosen a finite difference method. The steps leading to the difference formulation of the momentum equation shall be shown in detail as follows:

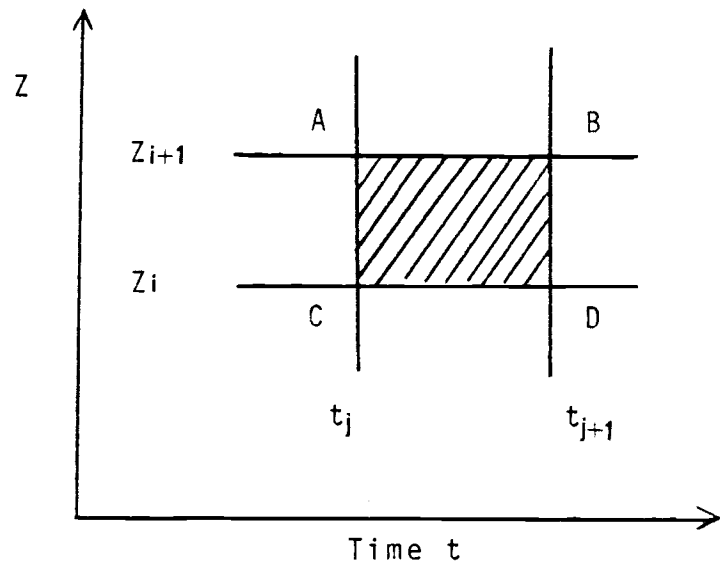

Figure 3-1 The Mesh Points in Space-Time Coordinate System

We integrate equation 2-2 from z(i), t(j), to z(i+1), t(j+1), as demarked by points A, B, C, D in Figure 3-1. Using indices (i,j) to represent a quantity pertaining to [z(i),t(j)] , we get

$$\int_{z_i}^{z_{i+1}}\int_{t_j}^{t_{j+1}} \frac{\partial}{\partial t} G\,dt\,dz = \int_{t_j}^{t_{j+1}}\int_{z_i}^{z_{i+1}} \left(-\frac{\partial P}{\partial z} + R\right)dz\,dt \qquad (3\text{-}5)$$

We use the implicit method for the time integration and trapezoidal rule to carry out the spatial integration of equation 3-5 term by term[10] . We obtain

$$LHS = \int_{z_i}^{z_{i+1}} [G(z,j+1)-G(z,j)]\,dz$$

$$= [G(i+1,j+1)+G(i,j+1)-G(i+1,j)-G(i,j)]*\Delta z/2 \qquad (3\text{-}6)$$

$$RHS1 = -\int_{t_j}^{t_{j+1}} [P(i+1,t)-P(i,t)]\,dt$$

$$= \int_{t_j}^{t_{j+1}} [P(i,t)-P(i+1,t)]\,dt$$

$$= [P(i,j+1)-P(i+1,j+1)]*\Delta t \qquad (3\text{-}7)$$

$$RHS2 = \int_{t_j}^{t_{j+1}}\int_{z_i}^{z_{i+1}} R\,dz\,dt$$

$$= \int_{t_j}^{t_{j+1}}\int_{z_i}^{z_{i+1}} \left[\left(\frac{\partial P}{\partial z}\right)_{acc} + \left(\frac{\partial P}{\partial z}\right)_{frict} + \left(\frac{\partial P}{\partial z}\right)_{grav}\right]dz\,dt \qquad (3\text{-}8)$$

where

LHS = left hand side of equation 3-5

RHS1= first term of right hand side of equation 3-5

RHS2= second term of right hand side of equation 3-5

The integration of acceleration, wall friction and gravitational force can be accomplished from equations 3-2 through 3-4. These terms will be defined separately below. The acceleration term in equation 3-8 is derived from the definition in equation 3-2. The pressure drop in difference form becomes

$$\int_{t_j}^{t_{j+1}} \int_{z_i}^{z_{i+1}} \left(\frac{\partial P}{\partial z}\right)_{acc} dz dt$$

$$= -\int_{t_j}^{t_{j+1}} \left[\frac{G^2}{\rho}(i+1,t) - \frac{G^2}{\rho}(i,t)\right] dt$$

$$= -\left[\frac{G^2}{\rho}(i+1,j+1) - \frac{G^2}{\rho}(i,j+1)\right] * \Delta t \qquad (3\text{-}9)$$

From equation 3-3, the discrete pressure gradient term due to channel wall friction is given by

$$\int_{t_j}^{t_{j+1}} \int_{z_i}^{z_{i+1}} \left(\frac{\partial P}{\partial z}\right)_{frict} dz dt$$

$$= \int_{t_j}^{t_{j+1}} \int_{z_i}^{z_{i+1}} - \frac{2fG^2}{\rho Dh} dzdt$$

$$= - \frac{2}{Dh} [\frac{fG^2}{\rho}(i+1,j+1) + \frac{fG^2}{\rho}(i,j+1)] * \Delta z * \Delta t/2$$

$$= - [\frac{fG^2}{\rho}(i+1,j+1) + \frac{fG^2}{\rho}(i,j)] \Delta t \Delta z/Dh \qquad (3\text{-}10)$$

From equation 3-4, the pressure gradient term due to the gravitational force is given by

$$\int_{t_j}^{t_{j+1}} \int_{z_i}^{z_{i+1}} (\frac{\partial P}{\partial z})_{grav} dzdt$$

$$= - \int_{t_j}^{t_{j+1}} \int_{z_i}^{z_{i+1}} (\rho * g) dzdt$$

$$= - \frac{g}{2} [\rho(i+1,j+1) + \rho(i,j+1)] \Delta t \Delta z \qquad (3\text{-}11)$$

Substituting equation 3-9, 3-10, 3-11 into equation 3-8 and setting

$$LHS = RHS1+RHS2$$

we get

$$P(i+1,j+1) = P(i,j+1)-\Delta Pg-\Delta Pa-\Delta Pf-\Delta Pt \qquad (3\text{-}12)$$

where

$$\Delta Pa = \left[\frac{G^2}{\rho}(i+1,j+1) - \frac{G^2}{\rho}(i,j+1)\right] \qquad (3\text{-}13)$$

$$\Delta Pf = \left[\frac{G^2 f}{\rho}(i+1,j+1) + \frac{G^2 f}{\rho}(i,j+1)\right] * \Delta z / Dh \qquad (3\text{-}14)$$

$$\Delta Pg = [\rho(i+1,j+1) + \rho(i,j+1)] * \Delta z * g/2 \qquad (3\text{-}15)$$

$$\Delta Pt = [G(i+1,j+1) + G(i,j+1) - G(i+1,j) - G(i,j)] * \Delta z / (2 * \Delta t) \qquad (3\text{-}16)$$

In addition to the above pressure drop components, another kind of pressure drop is considered. It represents the pressure drop due to a localized obstruction, such as spacer grids in the secondary flow path[11] . This component is written as

$$\Delta Ps = K * G**2/\rho \qquad (3\text{-}17)$$

where K is a constant characterizing the particular obstruction. Using the equation above we can write the momentum balance equation in terms of pressure differences as

$$P(i+1,j+1) = P(i,j+1) - \Delta Pg - \Delta Pa - \Delta Pf - \Delta Pt - \Delta Ps \qquad (3\text{-}18)$$

This equation is coupled to the other conservation equations (for mass and energy) and the state equations through the variables ρ, G, P, etc. Solution of these equations is performed by an iteration procedure which is presented in Appendix D.

In order to satisfy the boundary condition P2o on the secondary side, we use Newton's method (see Appendix C) to find an estimate of the inlet pressure, that is

$$P2i^{(n+1)} = P2i^{(n)} + [PE-P2o^{(n)}]*[P2i^{(n)}-P2i^{(n-1)}]/[P2o^{(n)}-P2o^{(n-1)}] \quad (3\text{-}19)$$

where PE is the boundary condition (outlet pressure of secondary side); the superscript n represents the iteration index. So, in calculating the secondary side, we have two iteration loops, an inner iteration loop for solving the nodal conservation and state equations, and an outer iteration loop to find the secondary inlet pressure.

4. FRICTION FACTOR AND BAROCZY MODEL

The friction coefficient f used in equation 3-3 is obtained for three different cases as below:

4.1. Single-phase, Fully Developed Laminar Flow

For circular channels, the laminar friction factor has been calculated theoretically[12]. The result is

$$f = 16/Re \tag{4-1}$$

where Re is the Reynolds number which is defined as

$$Re = G*Dh/\mu \tag{4-2}$$

where

μ = viscosity

G = mass flow rate

Dh= equivalent diameter

Usually, flow conditions with Re less than 2300 are defined as laminar flow and Re greater than 2300 as turbulent flow.

4.2. Single-phase, Fully Developed Turbulent Flow

Many empirical formulas have been recommended for friction factor of the single-phase, fully developed turbulent flow[13]. In the NEW code, we adopt the approximate relationship

$$f = C*Re^{-0.2} \tag{4-3}$$

where C=0.064 for homogeneous flow in commercially available smooth tubes. This relation is in good agreement with the Moody chart for turbulent flow in channels with smooth surfaces. The constant, C is defined in a manner consistent with the definition of the Fanning friction factor.

4.3. Two-phase Flow

A general empirical correlation for calculating the two-phase frictional pressure drop has been developed by Baroczy[14]. His work may be considered as an extension of that of Lockhart and Martinelli[15] and Martinelli and Nelson[16], all of whom defined the two-phase pressure drop in terms of the single-phase pressure drop

$$(\Delta P/\Delta z)_{tp} = (\Delta P/\Delta z)_{lp} * \phi^2 \tag{4-4}$$

where

ϕ^2 = two-phase frictional pressure drop multiplier

$(\Delta P/\Delta z)_{tp}$ = two-phase pressure drop per unit length

$(\Delta P/\Delta z)_{lp}$ = single phase pressure drop obtained at same mass velocity when the fluid is saturated liquid.

Instead of using the pressure as an index for the two-phase multiplier, Baroczy defines the property index B as

$$B = \left(\frac{\mu_l}{\mu_v}\right)^{0.2} * \left(\frac{\rho_v}{\rho_l}\right)$$

where

μ_l = viscosity in saturated liquid

μ_v = viscosity in saturated vapor

ρ_l = density in saturated liquid

ρ_v = density in saturated vapor

The relation between the pressure and the property index B is shown in Figure 4-1 which can be approximated by

$$B = \text{EXP}\ [-7.93782+(8.70047E-5)*\ln(P)**4] \qquad (4-5)$$

where

P = pressure (Pa)

The approximation of the quantity B by the expression above is presented in Figure 4-1 and shown that it is quite accurate for 3E5 < P(Pa) < 2E7. By this property index, Baroczy was able to obtain a correlation for ϕ^2 which was independent of pressure, and he also observed that his correlation could be used with the gas-phase pressure drop $(\Delta P/\Delta z)_v$ by observing that

$$\frac{(\Delta P/\Delta z)_l}{(\Delta P/\Delta z)_v} = \left[\frac{(\mu_l/\mu_v)^{0.2}}{\rho_l/\rho_v}\right]$$

The Baroczy correlation for the two-phase friction multiplier has been developed from experimental data in REF(17,18) and is given in two sets of curves:

(1) A plot of the reference two-phase multiplier as a function of the property index B for the reference mass flow rate Gr=1356 Kg/sec-m^2 (=1.0E+6 lb/hr-ft^2). These curves and values are shown in Figure 4-2 and Table 4-1.

(2) Plots of a two-phase multiplier flow correction factor (Fg) as a function of the property index, quality and mass flow rate. The curves

and values for G=0.25*Gr, G=0.5*Gr, G=2*Gr and G=3*Gr are given in Figure 4-3 through 4-6 and Table 4-2 through 4-5, respectively. This correction factor is used to adjust the two-phase flow multiplier ϕ^2 whenever G deviates from Gr. That is

$$\phi^2 = \phi_r^2 * Fg \qquad (4\text{-}6)$$

The Baroczy correlation included in the NEW code has been modified in the following manner. Linear extrapolation is used for values of the mass flux less than 0.25*Gr, and linear interpolation is used for mass flux values between 0.25*Gr and 3.0*Gr. For mass fluxes greater than 3*Gr, the mass flux correction is obtained from

$$Fg = \frac{(Fg \text{ at } G=3xGr)^{(G/Gr-2)}}{(Fg \text{ at } G=2xGr)^{(G/Gr-3)}} \qquad (4\text{-}7)$$

The friction pressure drop is defined in equation 3-3. The corresponding relation in case of two-phase conditions, using the two-phase multiplier is obtained in a consistent manner as follows. Substituting the definition of pressure drop (i.e. equation 3-3) into the definition of two-phase

multiplier (i.e., equation 4-4), we get

$$\left(\frac{\Delta P}{\Delta z}\right)_{tp} = \left(\frac{\Delta P}{\Delta z}\right)_{lp} * \phi^2$$

$$= \frac{G^2 f_s \phi^2}{2 Dh \rho_l}$$

$$= \frac{G^2}{2Dh} * \left(\frac{\rho_{fs} \phi^2}{\rho_l}\right)$$

$$= \frac{G^2}{2Dh\rho} * ft \qquad (4\text{-}8)$$

where fs is the friction coefficient for the saturated fluid with the same mass flow rate, and ft is defined as

$$ft = fs * \phi^2 * (\rho/\rho_l) \qquad (4\text{-}9)$$

The final form of two phase friction coefficent can be written as

$$ft = fs * \phi_r^2 * Fg * (\rho/\rho_l) \qquad (4\text{-}10)$$

Table 4-1

Values of the Baroczy Two Phase Multiplier
at G = 1356 kg/sec-m^2

Property	Thermodynamic Quality									
Index B	0.0	.001	0.01	0.05	0.10	0.20	0.40	0.60	0.80	1.00
.001	1.0	2.11	8.80	33.50	68.00	150.00	330.00	690.00	1040.00	1000.00
.003	1.0	2.02	8.10	26.20	41.00	73.00	138.00	255.00	380.00	333.00
.005	1.0	1.97	7.10	22.00	31.00	53.00	91.00	160.00	245.00	200.00
.007	1.0	1.83	5.90	17.20	25.00	42.00	68.00	116.00	175.00	143.00
.009	1.0	1.69	5.10	14.00	21.00	35.70	56.00	93.00	140.00	111.00
.010	1.0	1.60	4.70	12.80	19.20	33.00	51.50	84.00	125.00	100.00
.030	1.0	1.14	1.88	4.60	7.60	13.20	20.50	30.00	39.00	33.30
.050	1.0	1.10	1.50	3.15	4.60	8.20	13.00	18.50	23.00	20.00
.070	1.0	1.08	1.35	2.55	3.60	5.80	9.30	13.30	16.00	14.30
.090	1.0	1.07	1.28	2.25	3.05	4.50	7.20	10.40	12.50	11.10
.100	1.0	1.07	1.26	2.12	2.82	4.20	6.60	9.40	10.80	10.00
.300	1.0	1.02	1.10	1.40	1.63	1.92	2.50	3.20	3.50	3.33
.500	1.0	1.02	1.06	1.20	1.31	1.45	1.64	1.93	2.10	2.00
.700	1.0	1.01	1.03	1.10	1.15	1.22	1.28	1.40	1.43	1.43
1.000	1.0	1.00	1.00	1.00	1.00	1.00	1.00	1.00	1.00	1.00

Table 4-2

Values of the Baroczy Two Phase Multiplier Ratio
at G = 339 kg/sec-m^2

Property	Thermodynamic Quality									
Index B	.0	.001	.01	.05	.10	.20	.40	.60	.80	1.00
.001	1.0	1.40	1.40	1.30	1.49	1.49	1.36	1.26	1.13	1.00
.003	1.0	1.19	1.19	1.06	1.44	1.44	1.27	1.16	1.11	1.00
.005	1.0	1.17	1.17	1.04	1.41	1.41	1.24	1.14	1.10	1.00
.007	1.0	1.17	1.17	1.08	1.39	1.39	1.25	1.14	1.10	1.00
.009	1.0	1.18	1.18	1.12	1.28	1.38	1.26	1.14	1.10	1.00
.010	1.0	1.18	1.19	1.14	1.38	1.38	1.27	1.15	1.09	1.00
.030	1.0	1.20	1.26	1.29	1.37	1.37	1.31	1.15	1.08	1.00
.050	1.0	1.21	1.30	1.37	1.41	1.41	1.33	1.16	1.08	1.00
.070	1.0	1.20	1.28	1.42	1.48	1.48	1.35	1.17	1.08	1.00
.090	1.0	1.18	1.25	1.45	1.55	1.55	1.37	1.17	1.08	1.00
.100	1.0	1.17	1.24	1.47	1.58	1.58	1.38	1.18	1.08	1.00
.300	1.0	1.09	1.11	1.40	1.59	1.59	1.31	1.15	1.05	1.00
.500	1.0	1.05	1.07	1.23	1.34	1.34	1.18	1.09	1.03	1.00
.700	1.0	1.03	1.04	1.12	1.18	1.18	1.09	1.05	1.02	1.00
1.000	1.0	1.00	1.00	1.00	1.00	1.00	1.00	1.00	1.00	1.00

Table 4-3

Values of the Baroczy Two Phase Multiplier Ratio
at G = 678 kg/sec-m^2

Property	Thermodynamic Quality									
Index B	.0	.001	.01	.05	.10	.20	.40	.60	.80	1.00
.001	1.0	1.21	1.29	1.21	1.28	1.27	1.20	1.16	1.09	1.00
.003	1.0	1.15	1.26	1.15	1.27	1.24	1.16	1.12	1.07	1.00
.005	1.0	1.13	1.25	1.13	1.26	1.23	1.16	1.11	1.07	1.00
.007	1.0	1.13	1.23	1.14	1.26	1.23	1.17	1.11	1.07	1.00
.009	1.0	1.12	1.22	1.15	1.25	1.23	1.18	1.11	1.07	1.00
.010	1.0	1.12	1.22	1.15	1.25	1.23	1.18	1.11	1.07	1.00
.030	1.0	1.11	1.18	1.19	1.23	1.24	1.22	1.20	1.08	1.00
.050	1.0	1.10	1.15	1.21	1.22	1.25	1.24	1.27	1.08	1.00
.070	1.0	1.09	1.14	1.23	1.25	1.30	1.25	1.32	1.08	1.00
.090	1.0	1.09	1.13	1.25	1.30	1.37	1.26	1.40	1.07	1.00
.100	1.0	1.09	1.12	1.26	1.31	1.40	1.27	1.42	1.07	1.00
.300	1.0	1.06	1.06	1.23	1.33	1.42	1.23	1.20	1.04	1.00
.500	1.0	1.04	1.04	1.13	1.19	1.24	1.13	1.07	1.03	1.00
.700	1.0	1.02	1.02	1.07	1.10	1.12	1.07	1.04	1.01	1.00
1.000	1.0	1.00	1.00	1.00	1.00	1.00	1.00	1.00	1.00	1.00

Table 4-4

Values of the Baroczy Two Phase Multiplier Ratio
at G = 2712 kg/sec-m^2

Property	Thermodynamic Quality									
Index B	.0	.001	.010	.050	.100	.200	.400	.600	.800	1.00
.001	1.0	.810	.700	.720	.730	.740	.790	.838	.920	1.00
.003	1.0	.850	.680	.700	.730	.750	.804	.855	.928	1.00
.005	1.0	.860	.690	.700	.730	.760	.800	.848	.919	1.00
.007	1.0	.870	.720	.720	.740	.760	.789	.830	.902	1.00
.009	1.0	.870	.730	.730	.750	.760	.778	.815	.893	1.00
.010	1.0	.870	.740	.730	.750	.760	.775	.810	.888	1.00
.030	1.0	.890	.820	.770	.790	.770	.731	.748	.840	1.00
.050	1.0	.900	.860	.790	.800	.780	.710	.720	.816	1.00
.070	1.0	.910	.880	.800	.800	.750	.700	.700	.795	1.00
.090	1.0	.930	.890	.790	.780	.722	.670	.670	.778	1.00
.100	1.0	.930	.890	.790	.770	.710	.660	.660	.770	1.00
.300	1.0	.970	.930	.830	.790	.728	.687	.687	.787	1.00
.500	1.0	.980	.960	.900	.880	.830	.814	.814	.875	1.00
.700	1.0	.990	.980	.950	.930	.920	.910	.910	.935	1.00
1.000	1.0	1.000	1.000	1.000	1.000	1.000	1.000	1.000	1.000	1.00

Table 4-5

Values of the Baroczy Two Phase Multiplier Ratio
at G = 4069 kg/sec-m^2

Property	Thermodynamic Quality									
Index B	.0	.001	.010	.050	.100	.200	.400	.600	.800	1.00
.001	1.0	.710	.550	.570	.610	.600	.680	.751	.835	1.00
.003	1.0	.760	.500	.520	.590	.614	.696	.776	.870	1.00
.005	1.0	.790	.510	.520	.600	.619	.686	.755	.852	1.00
.007	1.0	.800	.550	.550	.610	.620	.667	.727	.830	1.00
.009	1.0	.810	.580	.560	.620	.622	.650	.704	.811	1.00
.010	1.0	.810	.600	.570	.630	.623	.645	.695	.803	1.00
.030	1.0	.850	.730	.640	.670	.634	.580	.600	.725	1.00
.050	1.0	.870	.790	.680	.690	.640	.550	.560	.690	1.00
.070	1.0	.890	.820	.690	.690	.620	.530	.530	.663	1.00
.090	1.0	.900	.830	.690	.680	.600	.515	.515	.648	1.00
.100	1.0	.910	.840	.690	.680	.593	.510	.510	.640	1.00
.300	1.0	.960	.910	.770	.740	.670	.610	.610	.702	1.00
.500	1.0	.980	.950	.870	.850	.810	.775	.775	.830	1.00
.700	1.0	.990	.970	.930	.920	.900	.885	.885	.910	1.00
1.000	1.0	1.000	1.000	1.000	1.000	1.000	1.000	1.000	1.000	1.00

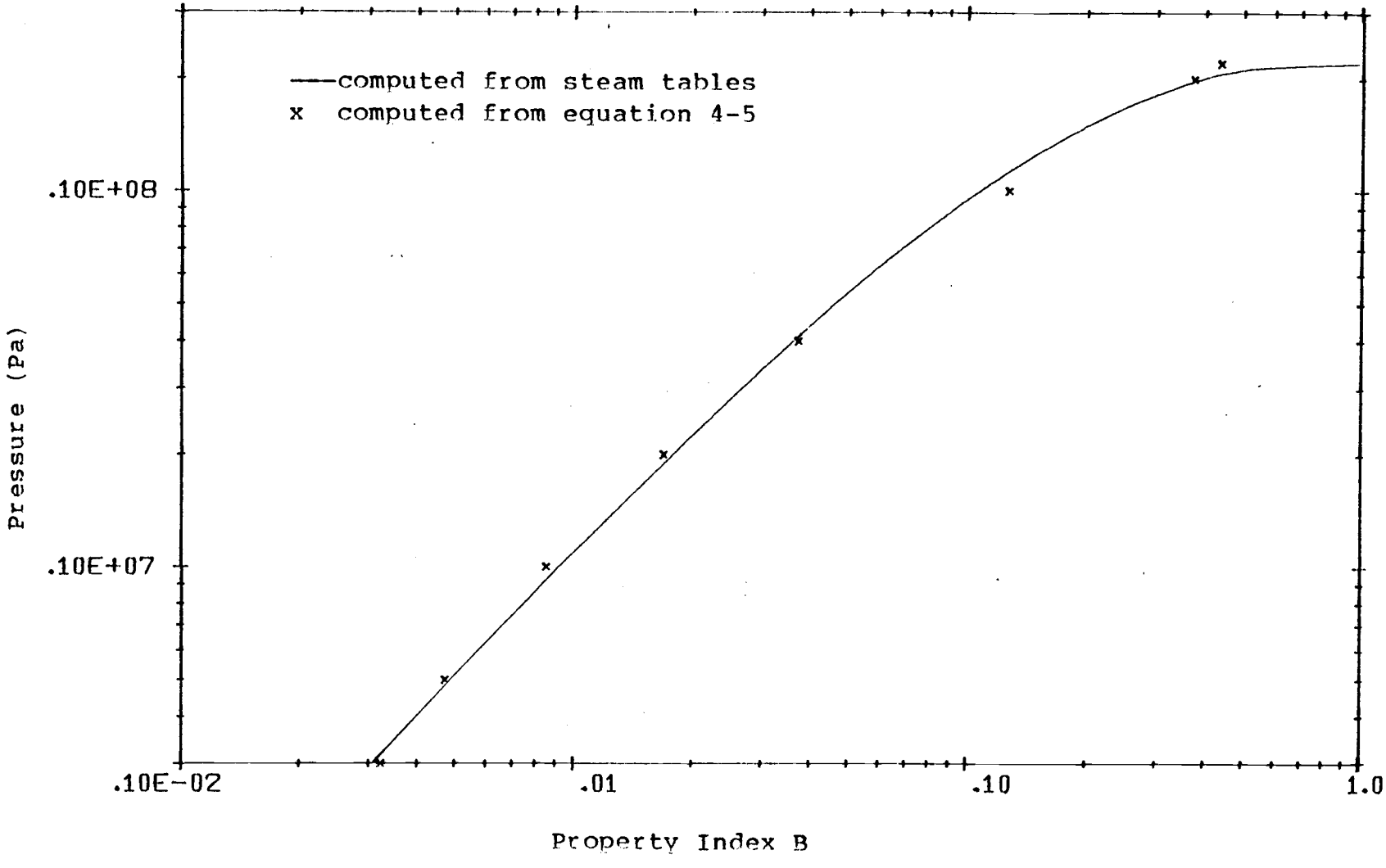

Figure 4-1 Dependency of Property Index B on Pressure P

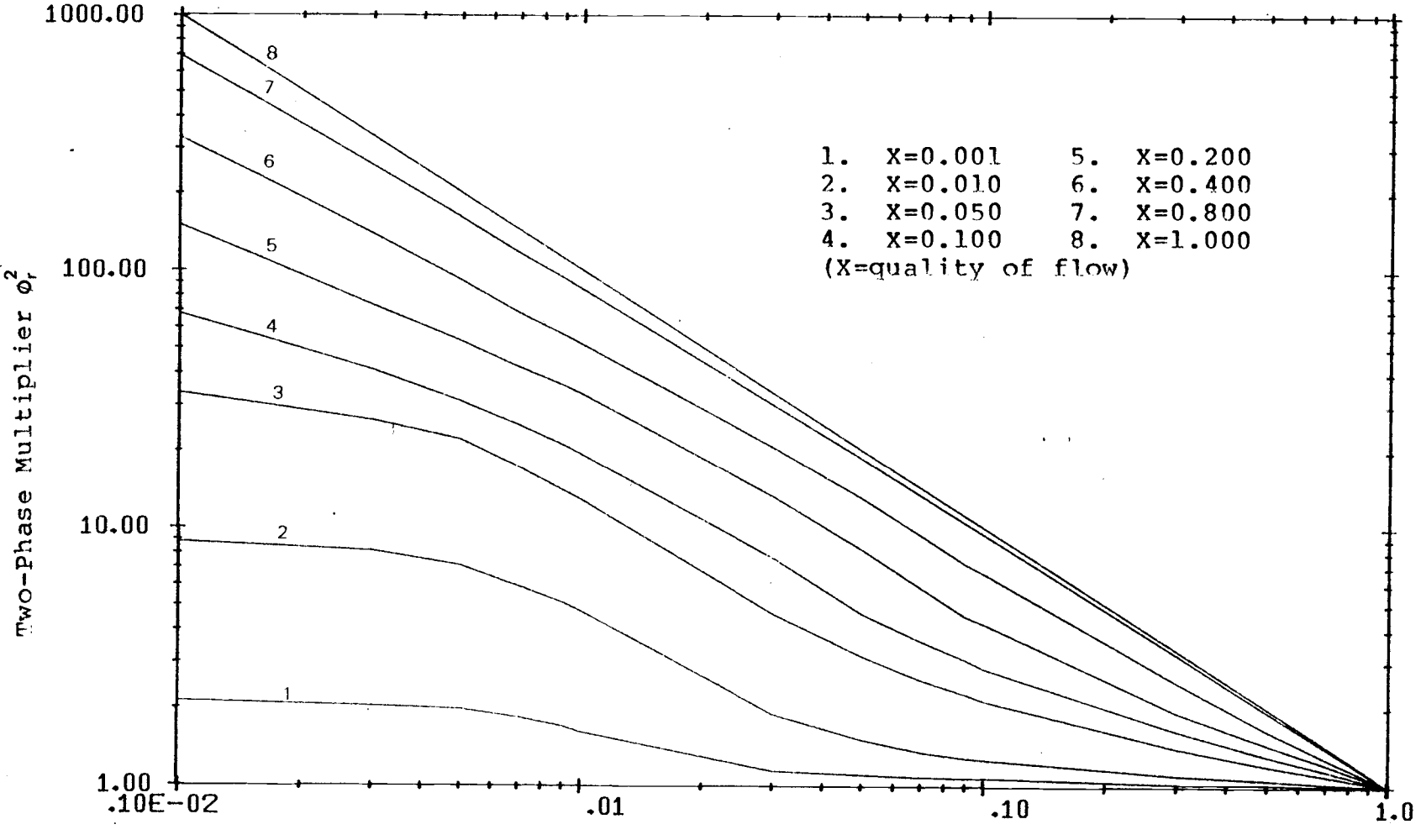

Figure 4-2 Baroczy Two-phase Multiplier ϕ_r^2 as a Function of the Property Index B

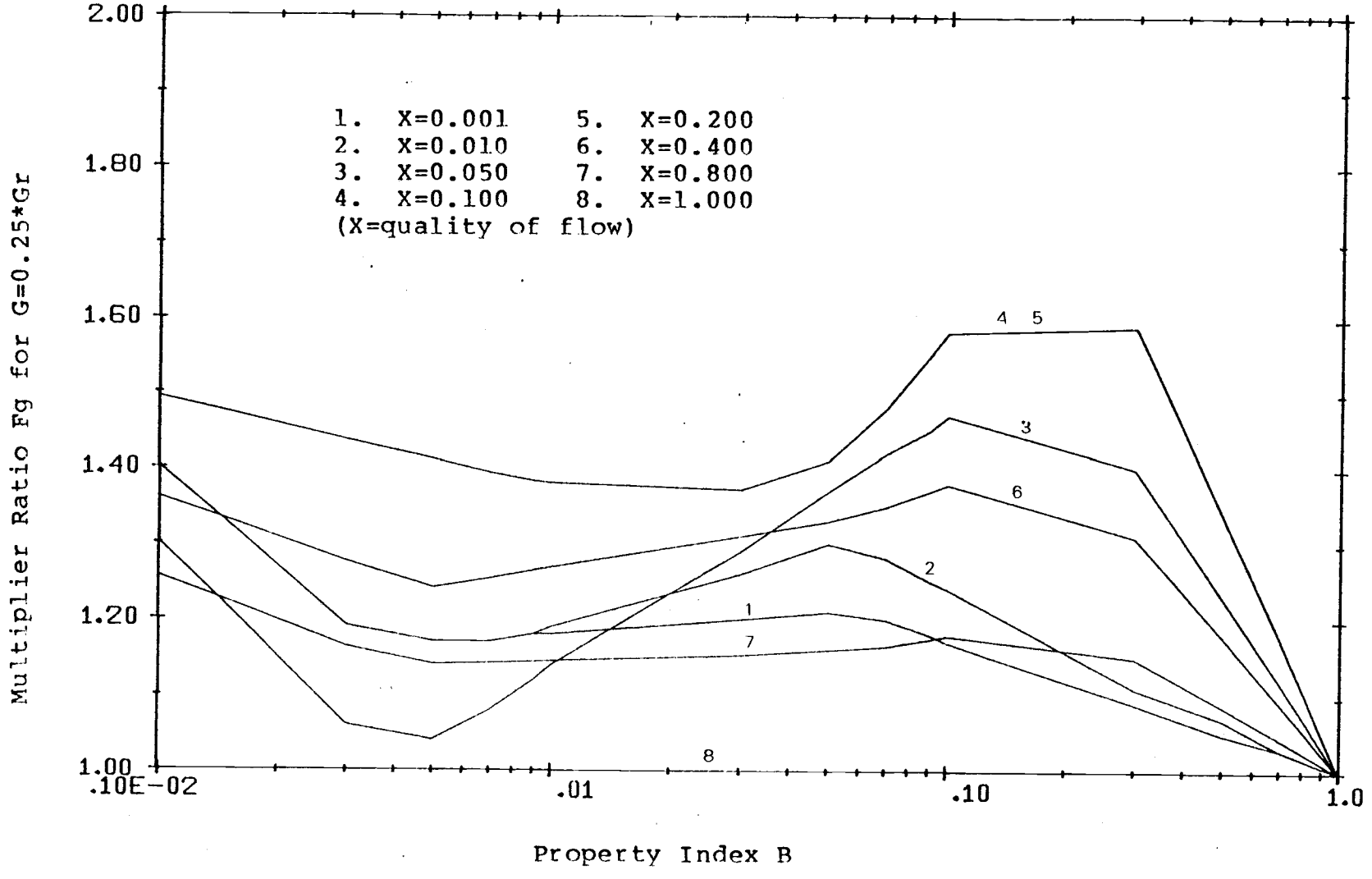

Figure 4-3 Baroczy Two-phase Multiplier Ratio, Fg
as a Function of the Property Index B

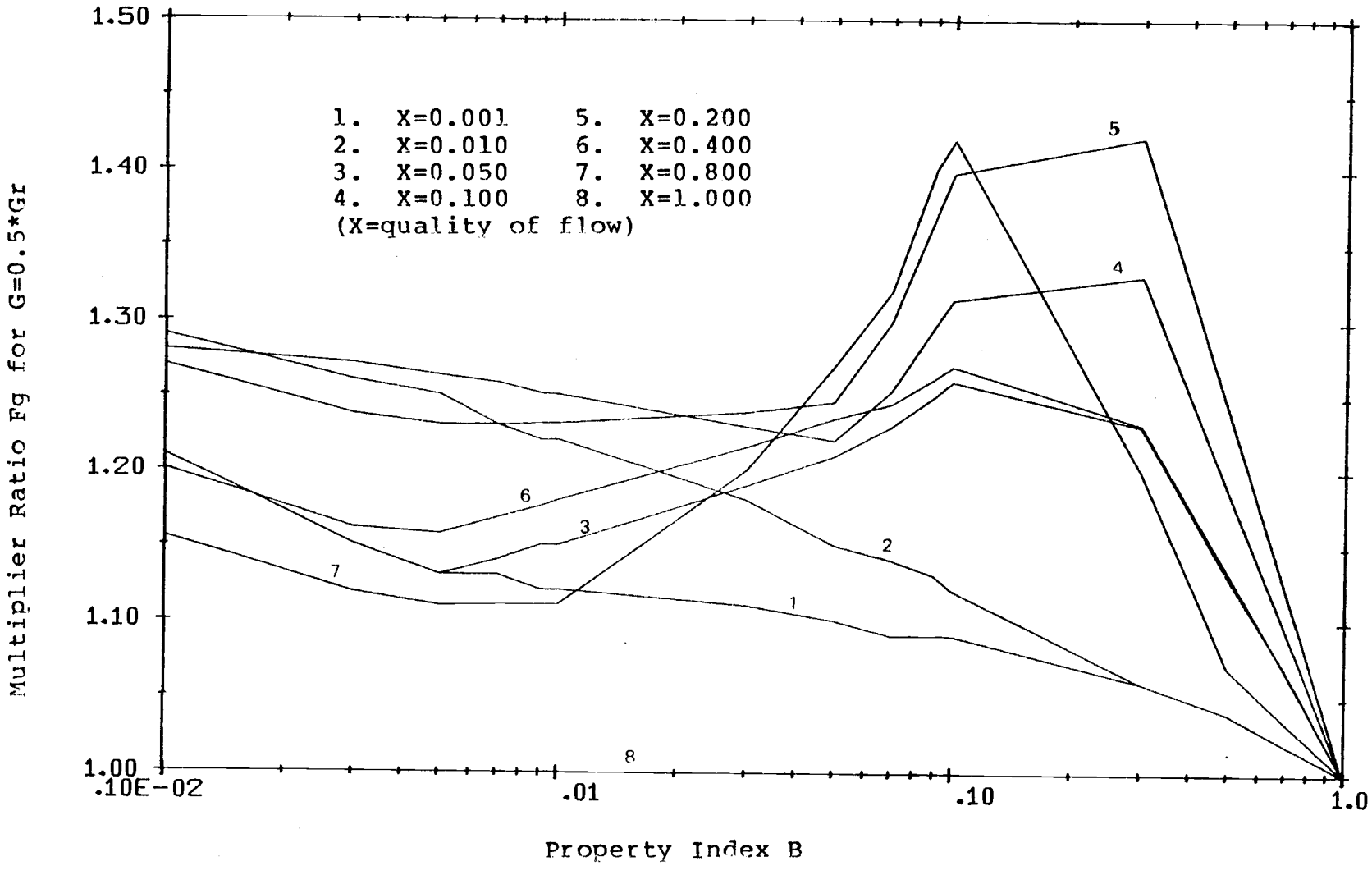

Figure 4-4 Baroczy Two-phase Multiplier Ratio, Fg
as a Function of the Property Index B

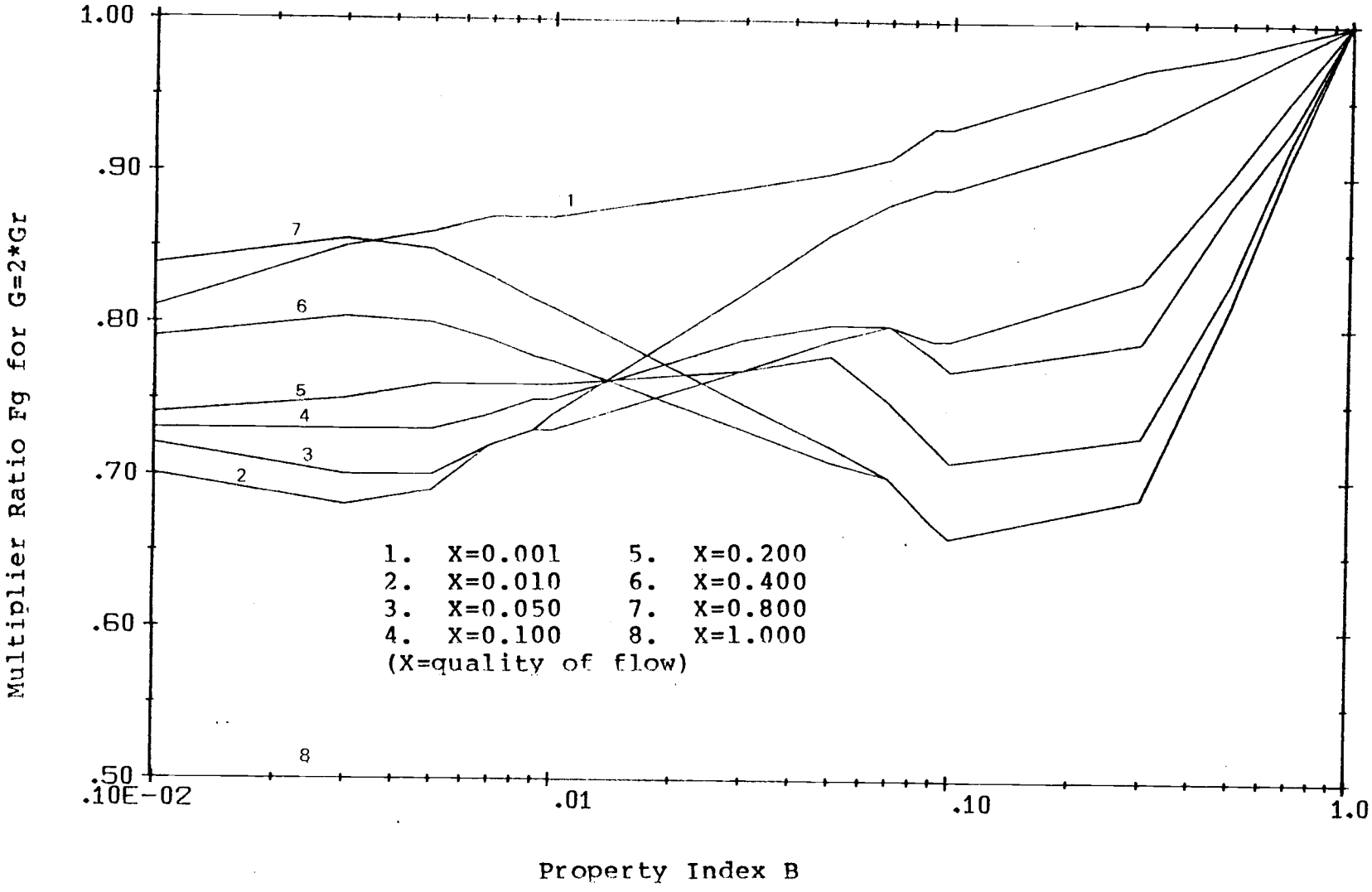

Figure 4-5 Baroczy Two-phase Multiplier Ratio, Fq
as a Function of the Property Index B

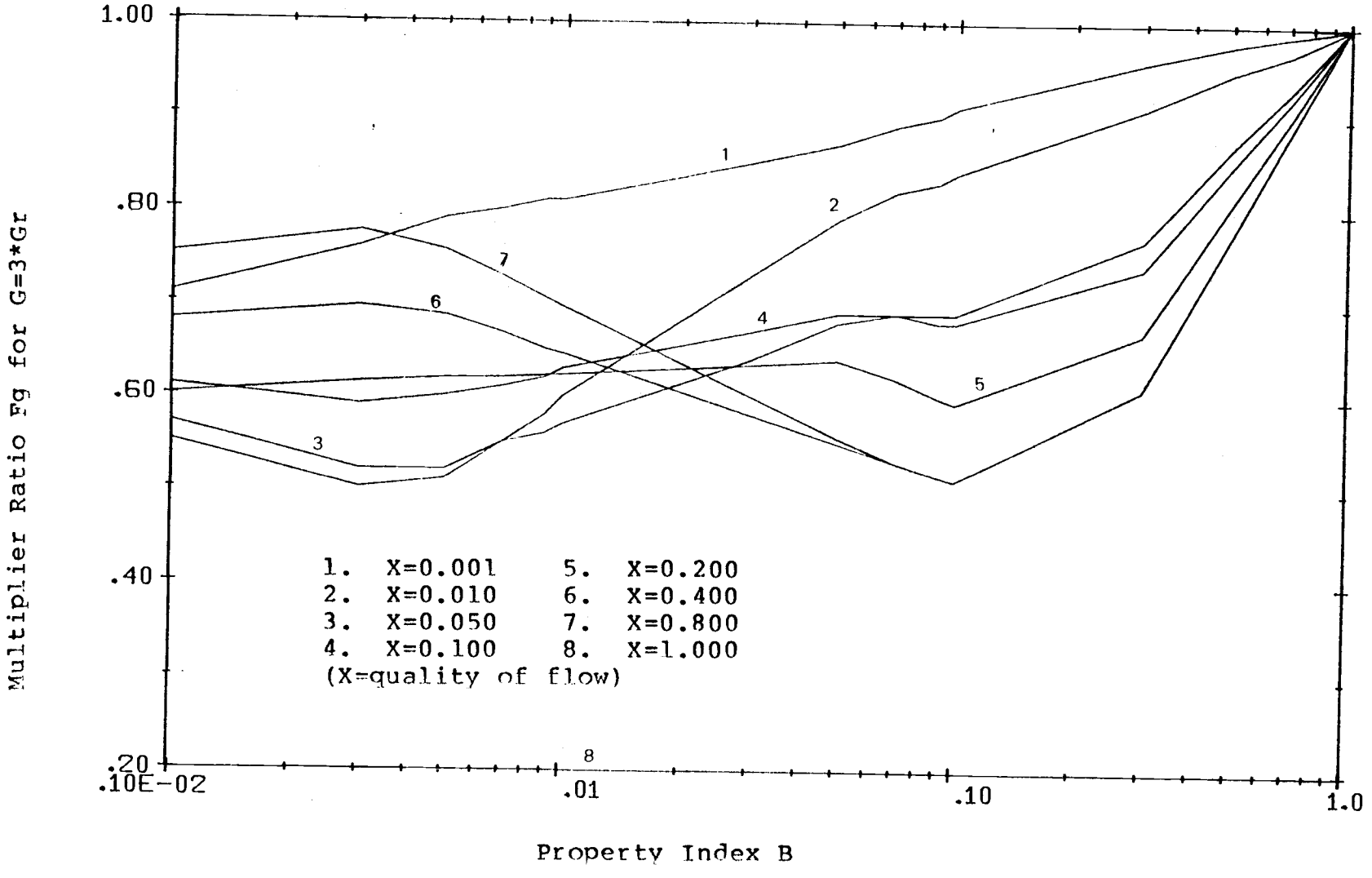

Figure 4-6 Baroczy Two-phase Multiplier Ratio, Fg as a Function of the Property Index B

5. RESULTS, DISCUSSION AND CONCLUSIONS

In order to verify the code it would be most desirable to compare results obtained from it with data measured on an OTSG. However, no such data were available. Substituting for this lack several cases were considered, as described in the following. In order to validate coding, to verify the models in a qualitative manner and to obtain experience with regard to integration and convergence parameters, comparisons were made against results obtained with the old version and with one case for which results obtained with a different code were available. The cases which are presented and discussed here shall be denoted as follows: DS represents a steady state case and DT1, DT2, DT3 and DT4 represent four different transient cases. The boundary conditions of these cases are shown in Table 5-1 through 5-3. Throughout this chapter the index n and Δt represent the number of mesh points for the spatial and the integration time interval, respectively.

5.1 Null-Transient

A null-transient is used to check the consistency between the steady state and the transient calculation. The time dependent boundary conditions of DT1 are kept

constant at values corresponding to DS for the first 5 seconds. The steady state pressure and enthalpy profile for the secondary side are shown in Figure 5-1a and 5-2a, respectively. Comparing the property profile for DT1 at t=5 seconds with that of DS, we find that none of the variables exhibits any significant drift.

5.2. Step Change in Feed Flow Rate

In the OLD code the steady state pressure profile must be given as input. Therefore a comparison of steady states calculated between the OLD and the NEW code is pointless.

The time dependent boundary conditions for case DT1 are selected such that all quantities are kept constant at their steady state values except G2i. Its value is assumed to drop to one half of the initial value at t=5 seconds and to promptly increase to twice the initial value at t=25 seconds. To study the behavior of the pressure drop during this transient, we compare the pressure profiles at 5, 25 and 45 seconds. As shown in the lines 1, 2 and 3 of Figure 5-1a, the total pressure drop (ΔP) increases with the increase of mass flow rate. With the same initial and boundary conditions, the pressure profiles from the OLD code are also shown in Figure 5-1a. Comparing with the pressure profiles of the NEW code, we find that the OLD code always over-estimates the transient response. For a

detailed study, the total pressure drop components (ΔPg , ΔPs , ΔPf , ΔPa and ΔPt) along the Z-direction are also shown in Figure 5-3 through 5-7 where the index number is the same as that used in Figure 5-1a. From these figures we find that over most of the expected operating range of mass flow rates the most important single pressure drop component is the gravitational pressure drop in the liquid region. Unlike the gravitational pressure drop, the other pressure drop components (i.e., ΔPs, ΔPf and ΔPa) are more significant in the vapor region than in the liquid region. The contribution of individual pressure drop components to the total pressure drop is shown in Table 5-4. Since the friction pressure drop is only about 10% of the total pressure drop, the assumption for the pressure drop model used in the OLD code (see section 2-2) is not a good approximation for transient calculations involving large changes in pressure drops and/or flow rates.

Because of the truncation or round-off error of G2, the pressure drop component ΔPt does not vanish for the null-transient (see equation 3-16). However, it is negligibly small compared with the other terms and does not cause any problem with regard to convergence.

The time variation of each component is also shown in Figures 5-8 and 5-9 where each component is expressed relative to its initial value ($\Delta Pj(t)/\Delta Pj(0)$). From this

figure we can see that the gravitational pressure drop experiences the smallest change of all pressure drop components with respect to the change of mass flow rate. The change of ΔPg comes from the change of density (see equation 3-16), rather than the change of mass flow rates. As shown in Figure 5-2a the enthalpy profile at 25 seconds (i.e., low G2i) is higher than that at 45 seconds (i.e., high G2i). Therefore, the density profile and the gravitational pressure drop at 25 seconds are smaller than these at 45 seconds.

From Figure 5-9 we also notice that ΔPt changes violently with the change of mass flow rates, however this pressure drop is still small compared with the total pressure drop. But it indeed causes a small peak (i.e., 5% of total pressure drop) in the total pressure drop at 5 and 25 seconds as shown on line 1 of Figure 5-8. Because of the density factor (see equations 3-14, 3-15 and 3-17) the rate of change of ΔPa, ΔPf and ΔPs is much smaller than that of the square of the mass flow rates. As indicated in Figure 5-8 and Figure 5-9 the prompt pressure drop change results from ΔPa, ΔPf, ΔPs and ΔPt, and the long term pressure drop change results from ΔPg.

It is interesting to point out that the total heat transfer rate increases by increasing the mass flow rates (see Figure 5-10) but the degree of superheat will decrease

(see line 3 of Figure 5-2a). This effect is undesirable with regard to turbine operation.

5.3. Sudden Loss of Feed Flow

The time dependent boundary conditions for case DT2 (see Table 5-2) are selected to simulate the loss of feed flow. All values at the boundaries are kept constant at steady state values except G2i which drops from 648 Kg/s to 1.0 Kg/s at t=0.2 seconds. The pressure and enthalpy profile after a 15 second transient calculation is shown in Figures 5-1b and 5-2b, respectively. Individual pressure drop components are also shown in Figures 5-3 through 5-7. These figures indicate that all pressure drop components approach zero except ΔPg which has a slight decrease. This demonstrates that for loss of feedwater flow conditions the gravitational pressure drop completely dominates the total pressure drop (90% of total).

The time variation of each pressure drop component ratio is also shown in Figure 5-11 where the indices are the same as in Figure 5-8. We notice that ΔPt again causes a small peak in the total pressure drop ratio. We also find that the pressure drop decreases abruptly at 0.2 seconds (because of the drop of ΔPa, ΔPf, ΔPs and ΔPt) and after that decreases continuously due to the change in the gravitational pressure drop ΔPg.

Another item of interest is that the heat transfer rate does not respond promptly with the drop of the inlet flow rate (see Figure 5-12). This is because a large inventory of fluid is stored in the steam generator. Therefore, there is no sudden decrease in heat transfer for this situation (i.e., loss of feed flow). However, there is an increase of primary outlet temperature as a result of the gradual reduction in heat removal from the primary side. Looking at the enthalpy profile, we find that the length of the two-phase region (main heat transfer region) tends to adjust so as to yield a nearly constant exit enthalpy.

5.4. Sudden Change in Feedwater Temperature

Case DT3 (see Table 5-2) is selected such that all boundary conditions are kept constant except T2i which drops from 237.8 (C) to 217.8 (C) in 0.4 seconds and increases to 257.8 (C) in 20 seconds. The pressure and enthalpy profile at 20 and 45 seconds are shown in Figure 5-1b and 5-2b, respectively. We find that the pressure drop decreases slightly with the decrease of T2i and increases slightly with the increase of T2i. Individual pressure drop components are shown separately in Figures 5-3 through 5-8. We find that ΔPg increases slightly with the decrease of T2i, but ΔPs and ΔPf decreases slightly

with the decrease of T2i.

The transients of pressure drop components relative to their initial values are shown in Figure 5-13 and 5-14. Although ΔPa changes significantly, it contributes only little to the total pressure drop. Because of the small change of ΔPg, the total pressure drop is fairly constant (see Figure 5-13). Conversely, the heat transfer rate is quite sensitive to the change of T2i (see Figure 5-10) because the heat transfer rate is proportional to the temperature gradient (see equation 2-7).

5.5 Comparing the NEW Code with the CADDS Code

The New code was applied to analyze the transients following a generator trip from 96% power at TMI-1. Measured transients of feed-flow and steam pressure are provided as time-dependent boundary conditions as shown in Table 5-3. This transient also has been simulated with the CADDS code. The CADDS code was developed by Babcock & Wilcox Co. the principal vendor of IEOTSGs, to analyze the IEOTSG behavior. No detail concerning the models used in CADDS were available nor was there any indication of the computing time required by that code. Figure 5-14 shows the transient heat-demand as calculated by the NEW code and the CADDS code. As we can see, they match quite well. Good agreement between these two codes for this case is

essential and provides some confidence that the NEW code will accurately predict other important transients.

5.6 Parametric Study with Regard to the Mesh Size

With an increase in the number of nodes on the space-time grid one expects to get higher accuracy at the expense of greater consumption of computer time. It is important to select an economic number of mesh points for an acceptable accuracy. We used the boundary conditions for case DT4 to cover a 10 second transient for several different mesh sizes. The selection of the number of mesh points, time steps and computer running time (CYBER 170 model 720) are shown in Table 5-5. The pressure and enthalpy profiles are shown in Figure 5-16 and 5-17. The heat transfer rate is also shown in Figure 5-15. Comparing these results we find that for the range n=25 to 50 and Δt=0.2 to 0.5 seconds the results agree quite well and therefore we conclude that for this case the solution is well converged with 25 nodes and Δt=0.5 seconds.

5.7. Conclusion and Future Work

This thesis has presented a detailed formulation of the momentum conservation equation and its implementation into a code for the description of an OTSG. The numerical solution techniques also are discussed. The results of

this model support the following conclusions:

(1) In the cases considered here the gravitational pressure drop constitutes the largest single component.

(2) Most of the gravitational pressure drop is contributed by the liquid region. This is because the density of fluid in the liquid region is much larger than that in other regions.

(3) For ΔPa, ΔPf and ΔPs, the pressure drop contributed by the vapor region is greater than that from the liquid region. This is because the velocity of fluid in the vapor region is much higher than that in other regions.

(4) The transient acceleration pressure drop (ΔPt) fluctuates strongly in transient calculations. However, since it is relatively small compared with other pressure drop components and dies away rapidly, it does not play an important role.

(5) The acceleration, friction and spacer pressure drops (ΔPa, ΔPf and ΔPs) respond promptly and significantly to the change of mass flow rates whereas the gravitational pressure drop responds quite slowly and relatively little to this type of perturbation. This is because ΔPs, ΔPf

and Pa is proportional to the square of fluid mass velocity, whereas the ΔP_g is proportional to the density of fluid.

(6) The exact values of the friction coefficients (f) are not of great significance with respect to the total pressure drop. Since the friction pressure drop is only about 10% of the total pressure drop, a 20% change in f only causes 2% change in total pressure drop.

(7) The change of inlet temperature has little effect on the pressure drop.

In summary, it has been shown that a detailed momentum equation is essential to accurately describe the pressure transient behavior of the OTSG in common transients such as were studied here.

For the time being, the NEW code only covers the tube-and-shell region of the steam generator. For more comprehensive studies the model can be expanded to include the nozzles, pipes, inlet region and outlet region. Furthermore in order to study the significance of subcooled boiling and slip between the liquid and the vapor, it may be of interest to investigate two-phase flow models other than the homogeneous equilibrium model which was used here.

Table 5-1

Boundary Condition for Steady State, Case DS

P1i(Pa)	T1i(C)	G1i(kg/s)	P2o(Pa)	T2i(C)	G2i(kg/s)
1.517E7	315.9	8717.9	6.378E6	237.8	648.83

Table 5-2

Time Dependent Boundary Conditions
for Cases DT1, DT2 and DT3

DT1		DT2		DT3	
t(sec)	G2i(kg/s)	t(sec)	G2i(kg/s)	t(sec)	T2i(C)
0.0	648.8	0.0	648.8	0.0	237.8
5.0	648.8	0.4	648.8	0.4	237.8
5.2	324.4	0.6	1.0	0.6	217.8
25.0	324.4	60.0	1.0	20.0	217.8
25.2	1297.6			20.2	257.8
60.0	1297.6			60.0	257.8

All other values are kept constant as shown in Table 5-1

Table 5-3

Time Dependent Boundary Conditions
for Case DT4

t (sec)	P1i (kPa)	t (sec)	T1i (C)	t (sec)	P2o (kPa)	t (sec)	G2i (kg/s)
0.0	151700	0.0	315.9	0.0	6378	0.0	648.8
1.0	152400	5.0	316.4	0.01	6378	0.01	648.8
4.5	16190	8.0	315.8	1.8	7254	2.0	545.3
5.0	16240	9.5	308.6	3.0	7378	4.0	591.4
6.0	16140	12.0	308.6	4.5	7461	5.6	431.4
10.0	15240	17.0	302.6	6.0	7391	10.4	214.7
11.0	14950	22.0	298.0	6.8	7420	13.0	320.3
16.0	14940	30.0	294.2	11.7	7250	19.4	162.8
26.0	14400	46.0	290.8	13.0	7191	27.4	162.8
33.0	14380	56.0	289.8	15.0	7212	56.0	488.9
43.0	14640			18.0	7143		
56.0	14640			56.0	6984		

All other values are kept constant as shown in Table 5-1

Table 5-4

Relative Contribution of Individual Pressure Drop Components, Case DT1

t(sec)	ΔPg/ΔP	ΔPs/ΔP	ΔPf/ΔP	ΔPa/ΔP	ΔPt/ΔP
5	60.12%	31.29%	6.57%	1.52%	0.45%
25	70.26%	22.39%	4.62%	0.94%	1.80%
45	47.68%	38.52%	10.03%	2.51%	1.25%

Table 5-5

Computing Time Requirement for Various Choices of Mesh Points
Case DT4 (0<t<10 sec.)

	n=25	n=50
t=0.2	36.3(sec)	63.5(sec)
t=0.5	19.5(sec)	31.5(sec)

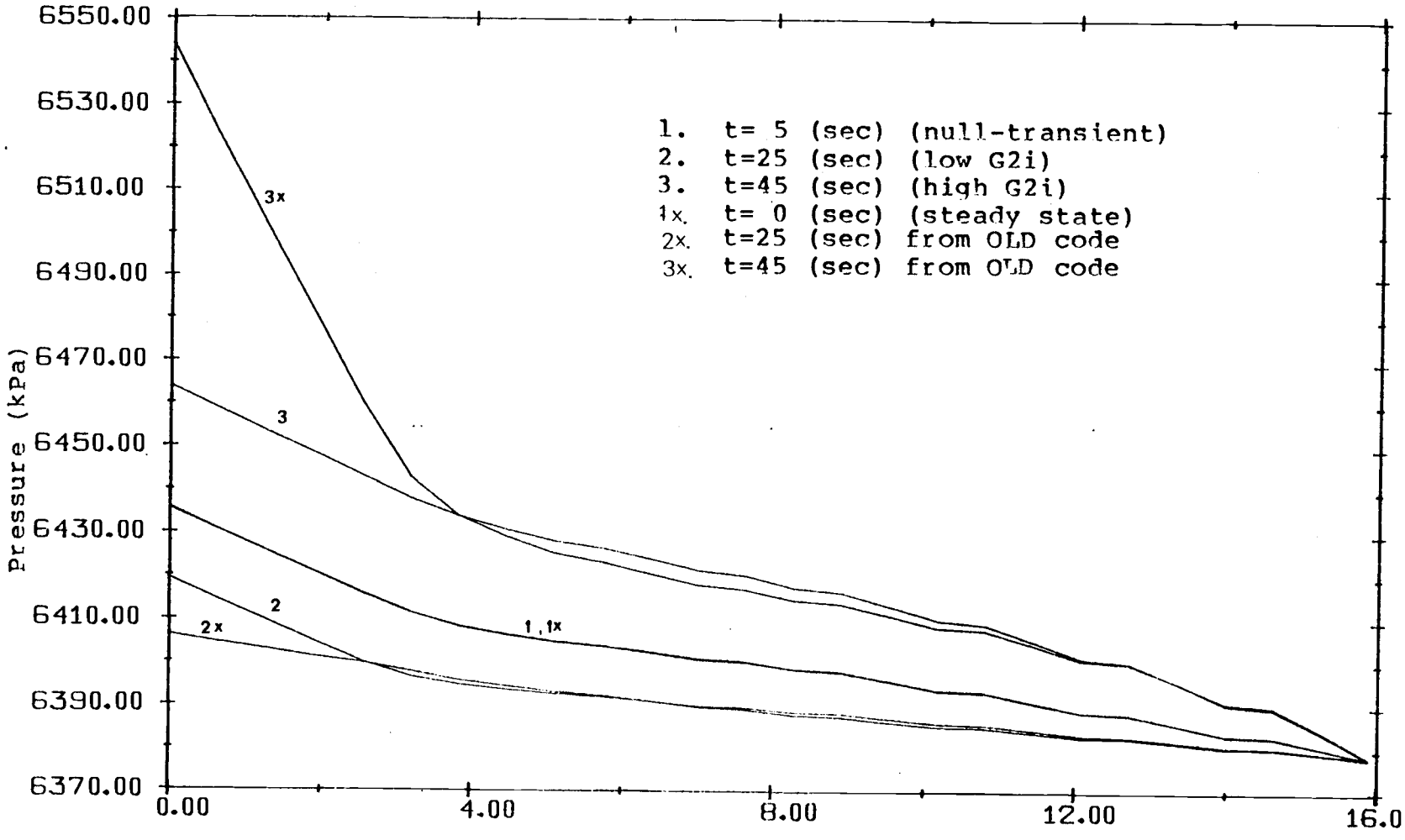

Distance from Bottom of Tube Bundle (m)

Figure 5-1a Pressure Profile for Case DT1

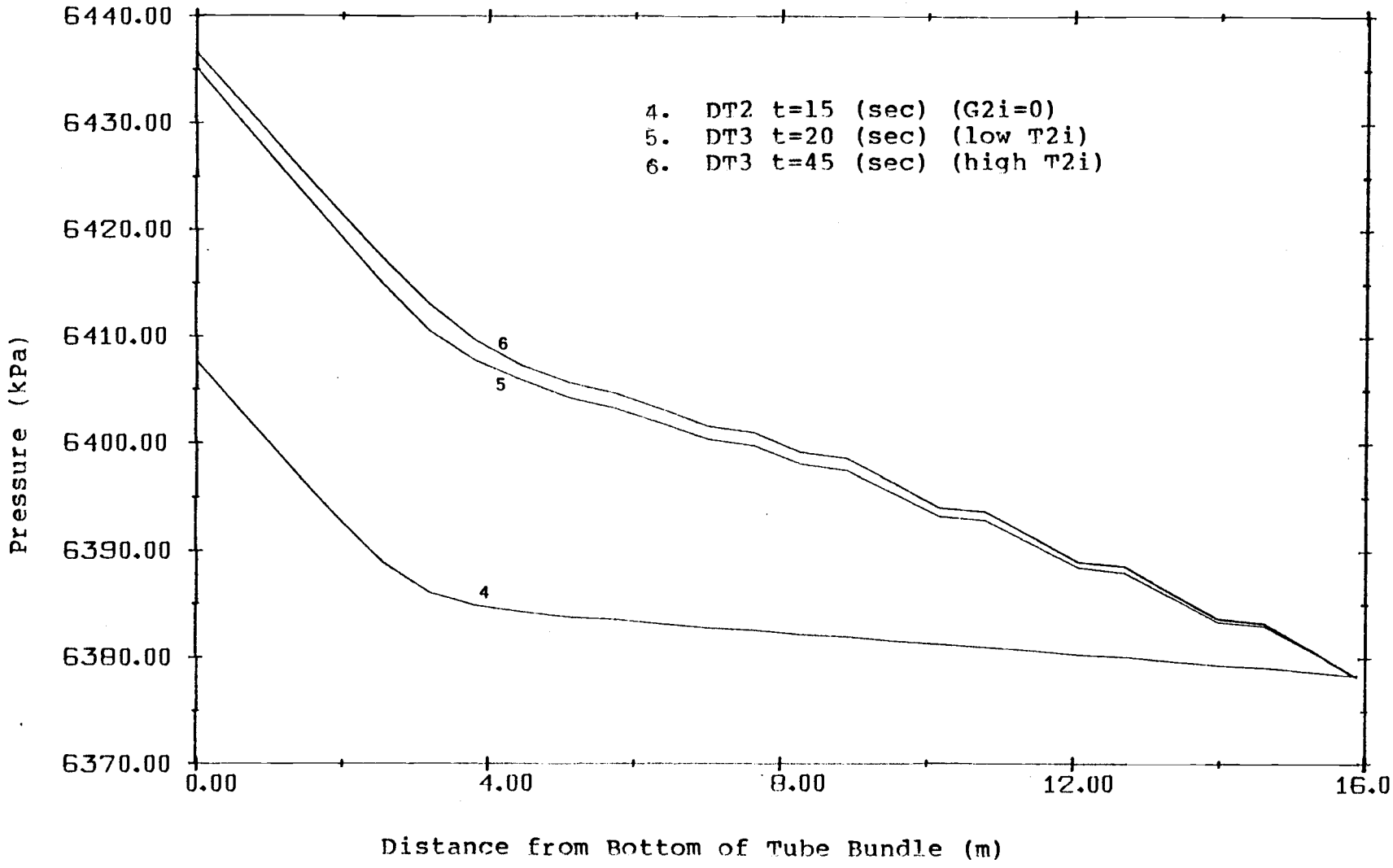

Figure 5-1b Pressure Profile for Cases DT2 and DT3

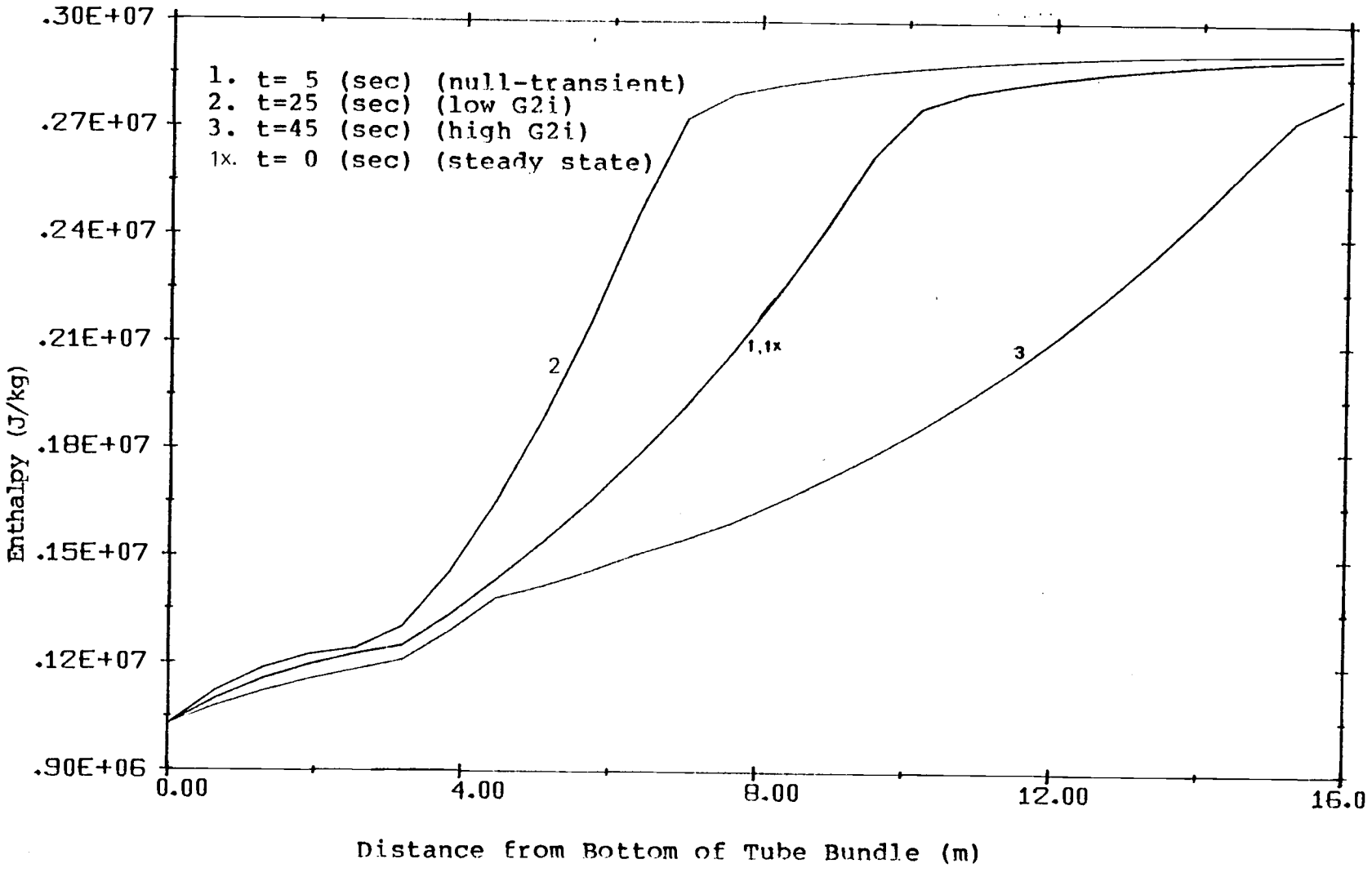

Figure 5-2a Enthalpy Profile for Case DT1

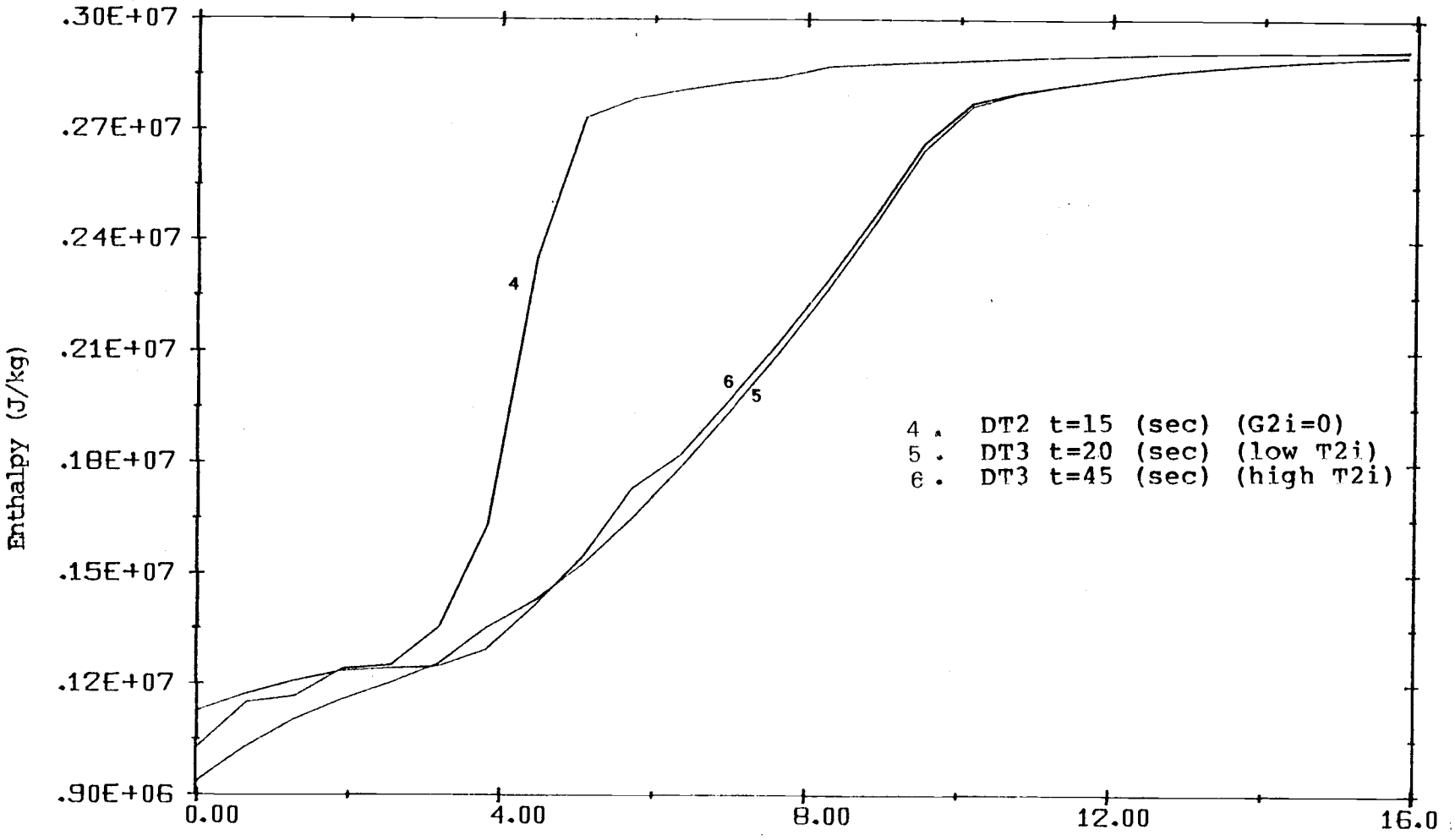

Figure 5-2b Enthalpy Profile for Cases DT2 and DT3

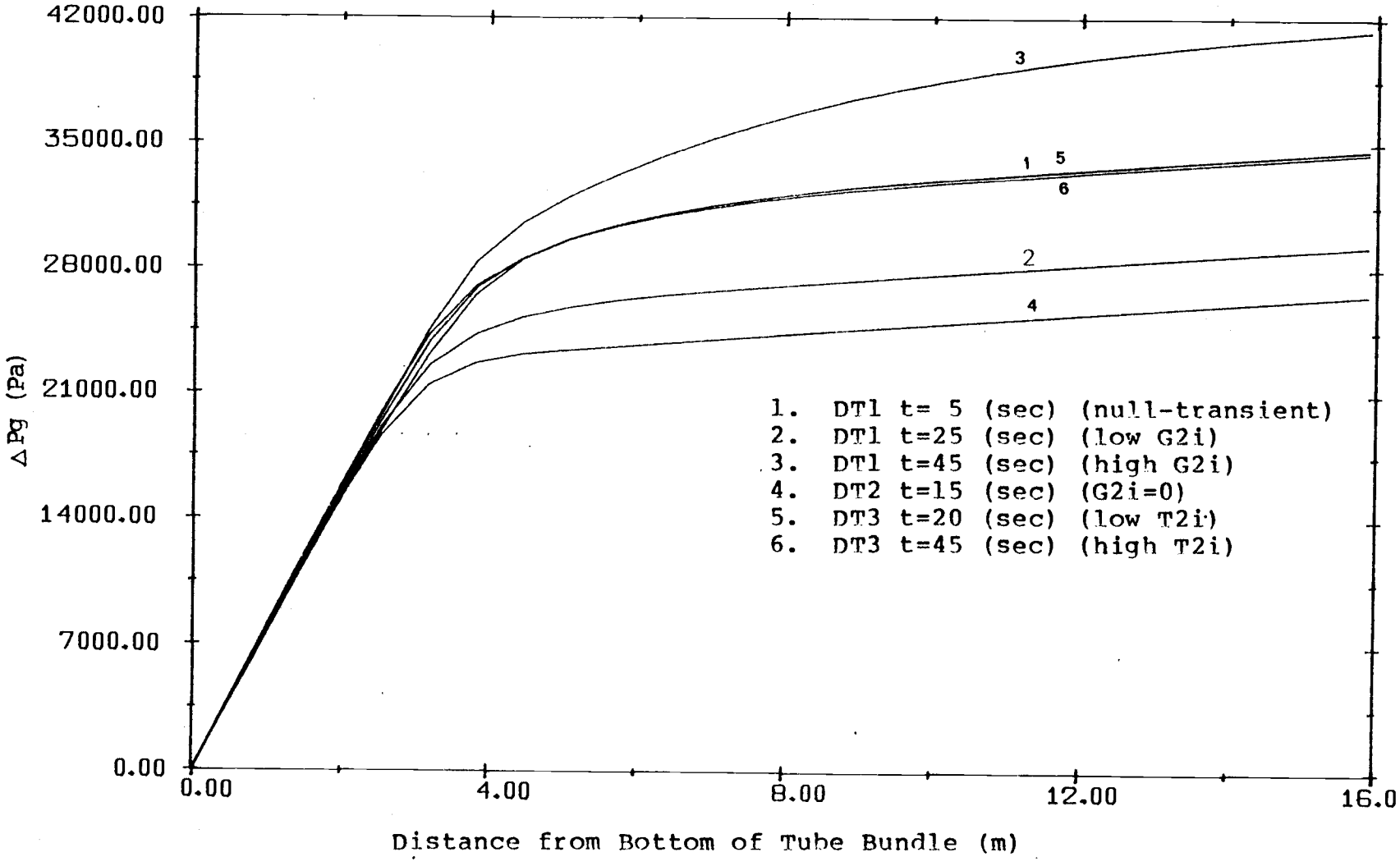

Figure 5-3 Profile of Gravitational Component of Pressure Drop, ΔPg for Cases DT1, DT2 and DT3

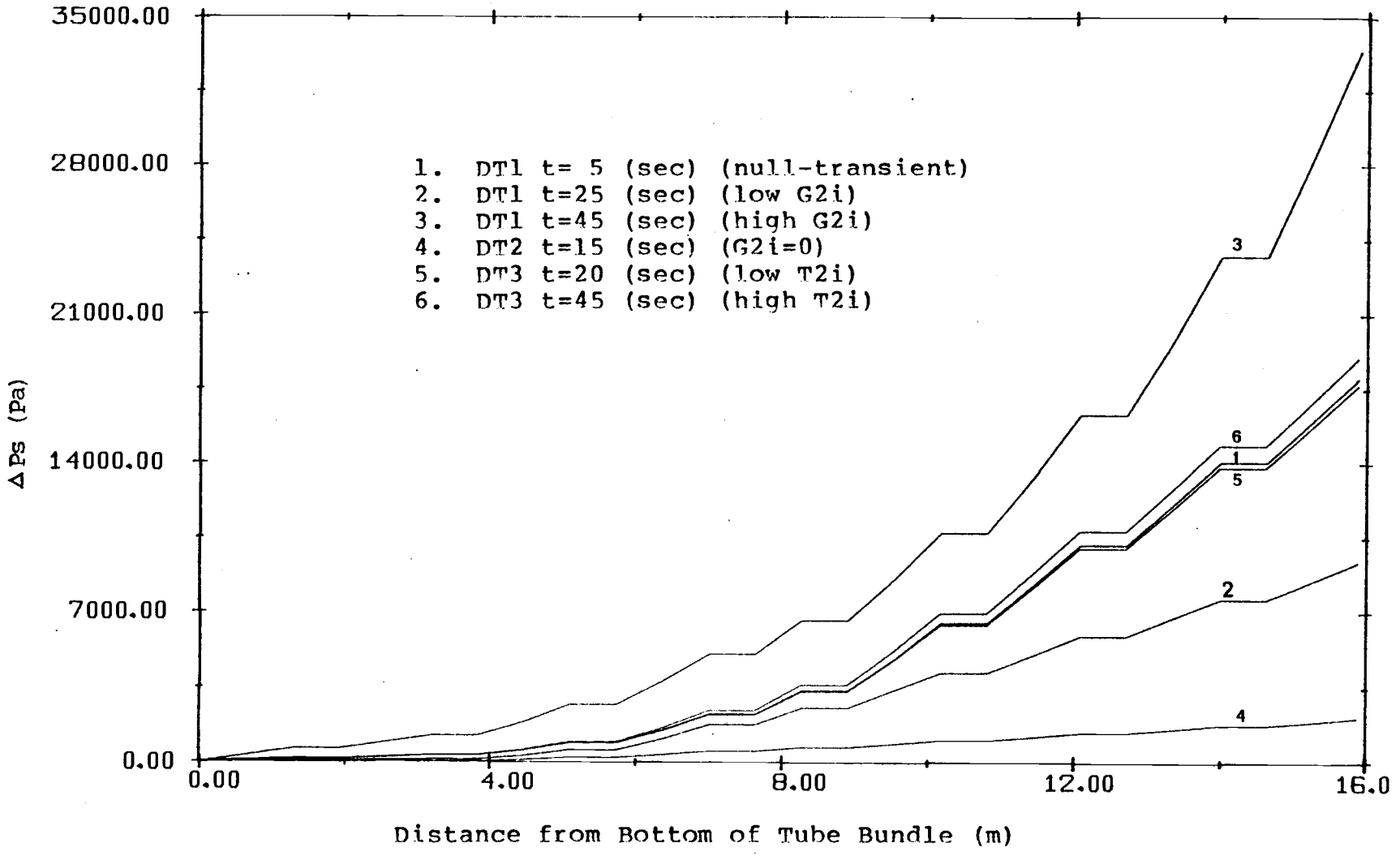

Figure 5-4 Profile of Spacer Component of Pressure Drop, ΔP_s for Cases DT1, DT2 and DT3

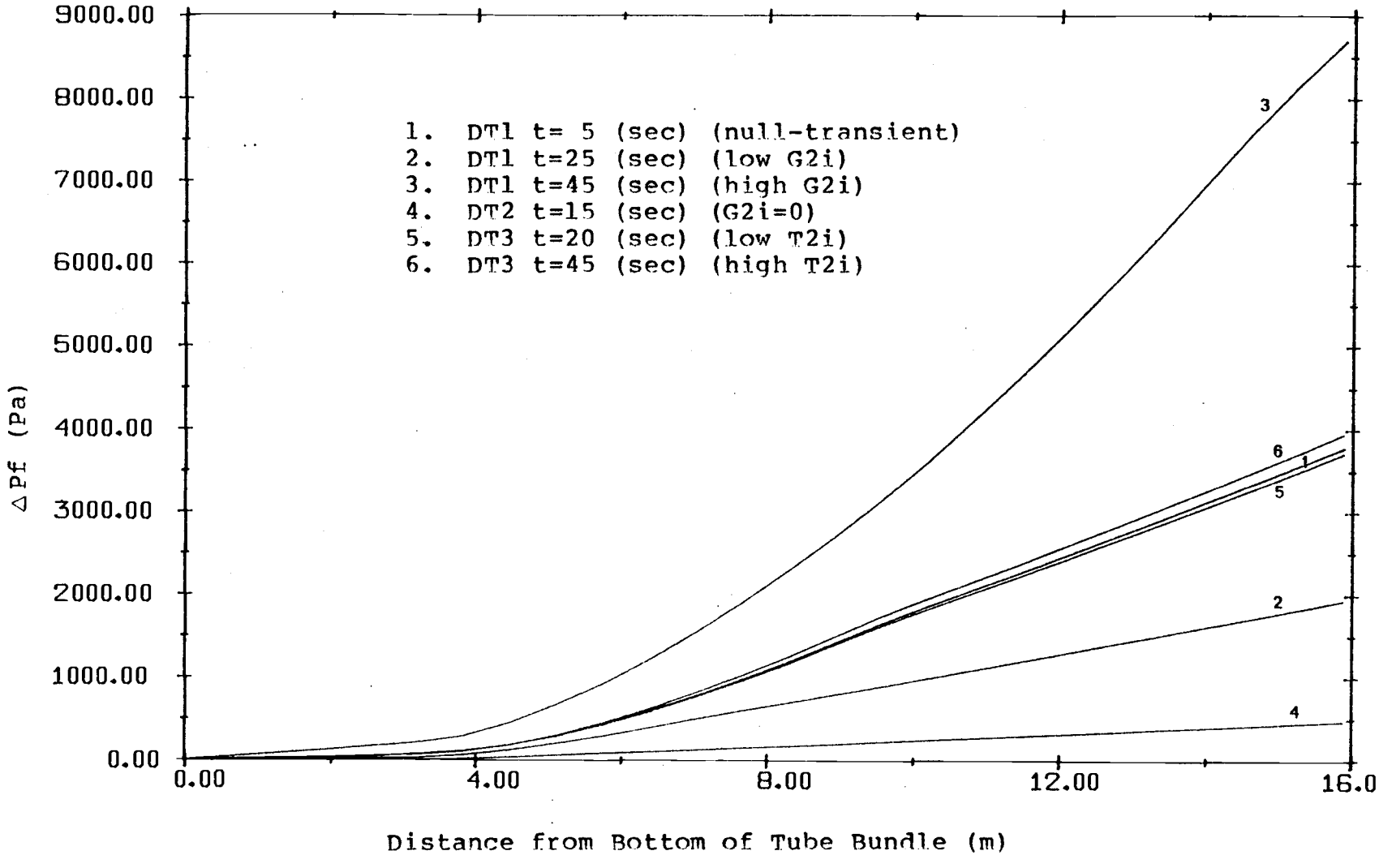

Figure 5-5 Profile of Friction Component of Pressure Drop, ΔP_f for Cases DT1, DT2 and DT3

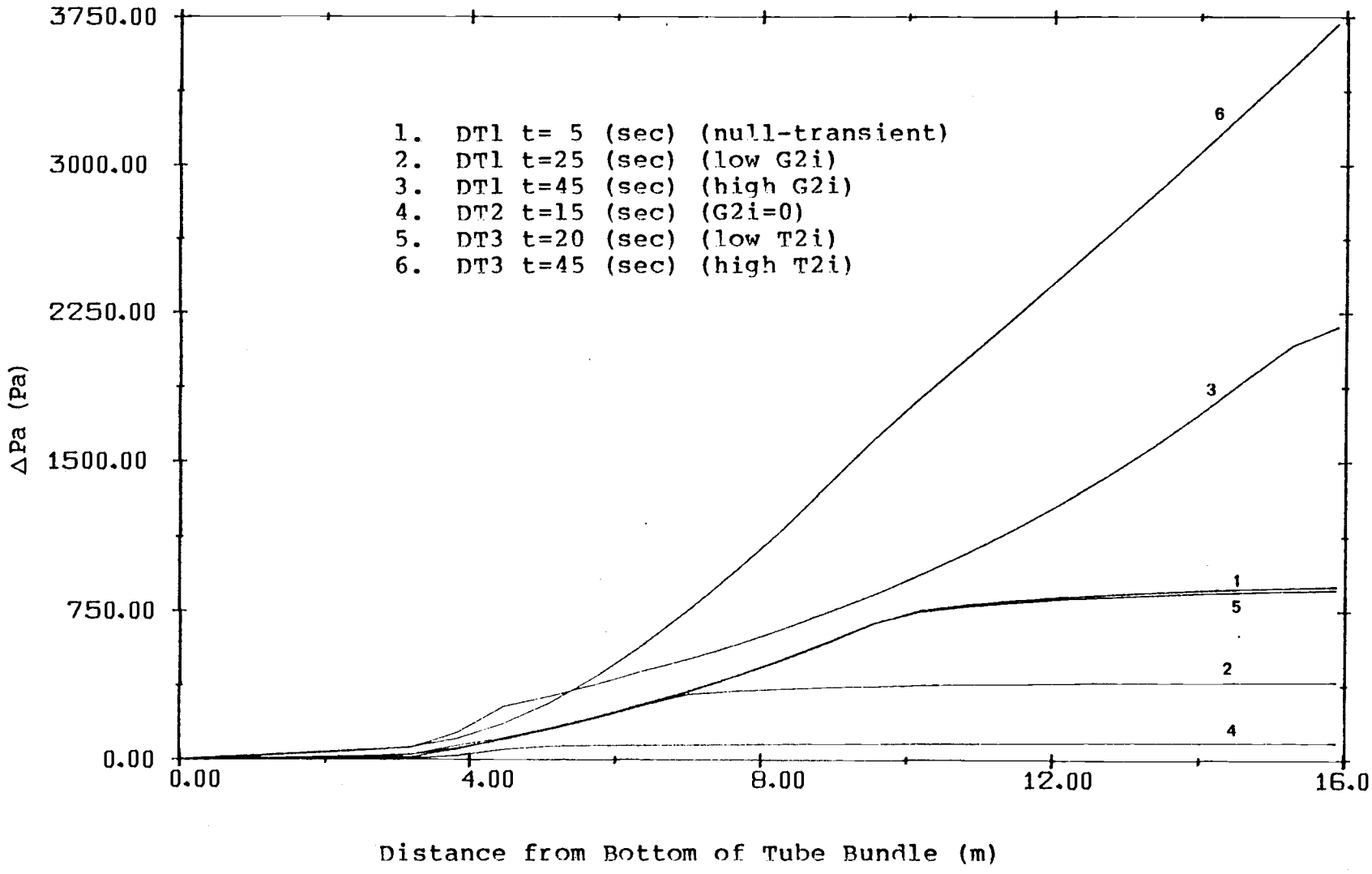

Figure 5-6 Profile of Acceleration Component of Pressure Drop, ΔPa for Cases DT1, DT2 and DT3

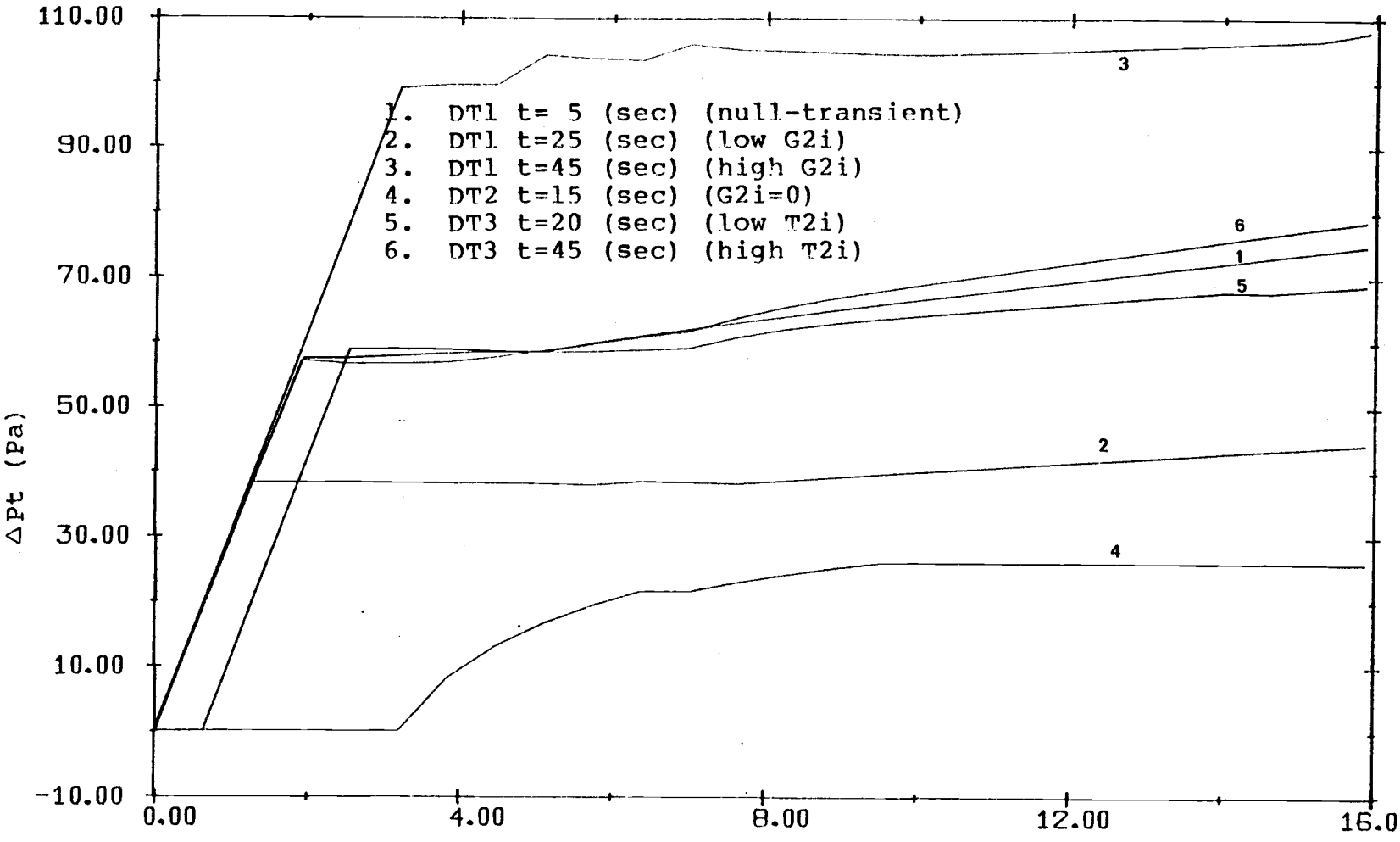

Figure 5-7 Profile of Transient Acceleration Component of Pressure Drop, ΔPt for Cases DT1, DT2 and DT3

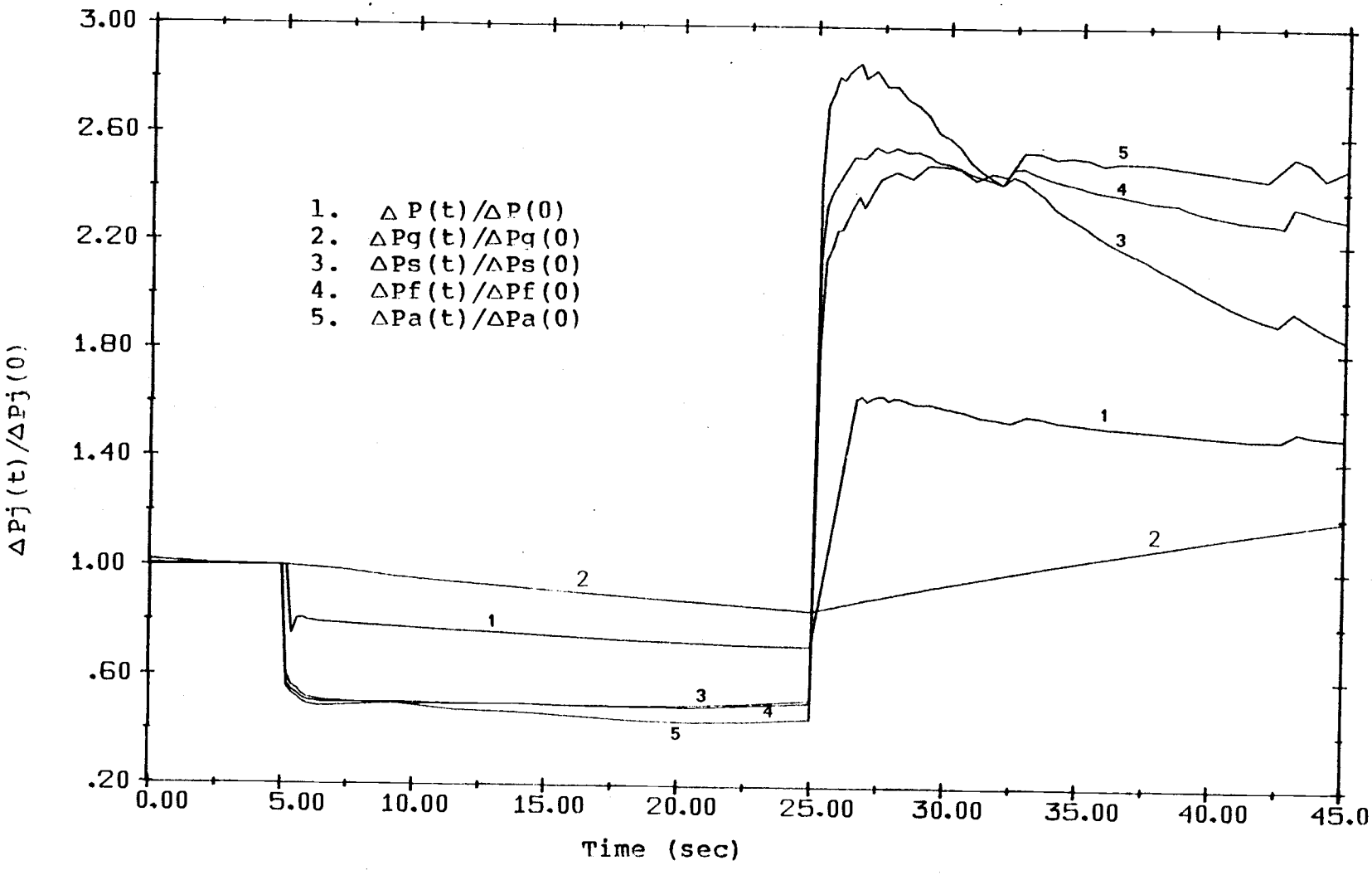

Figure 5-8 ΔPj(t)/ΔPj(0) for Case DT1

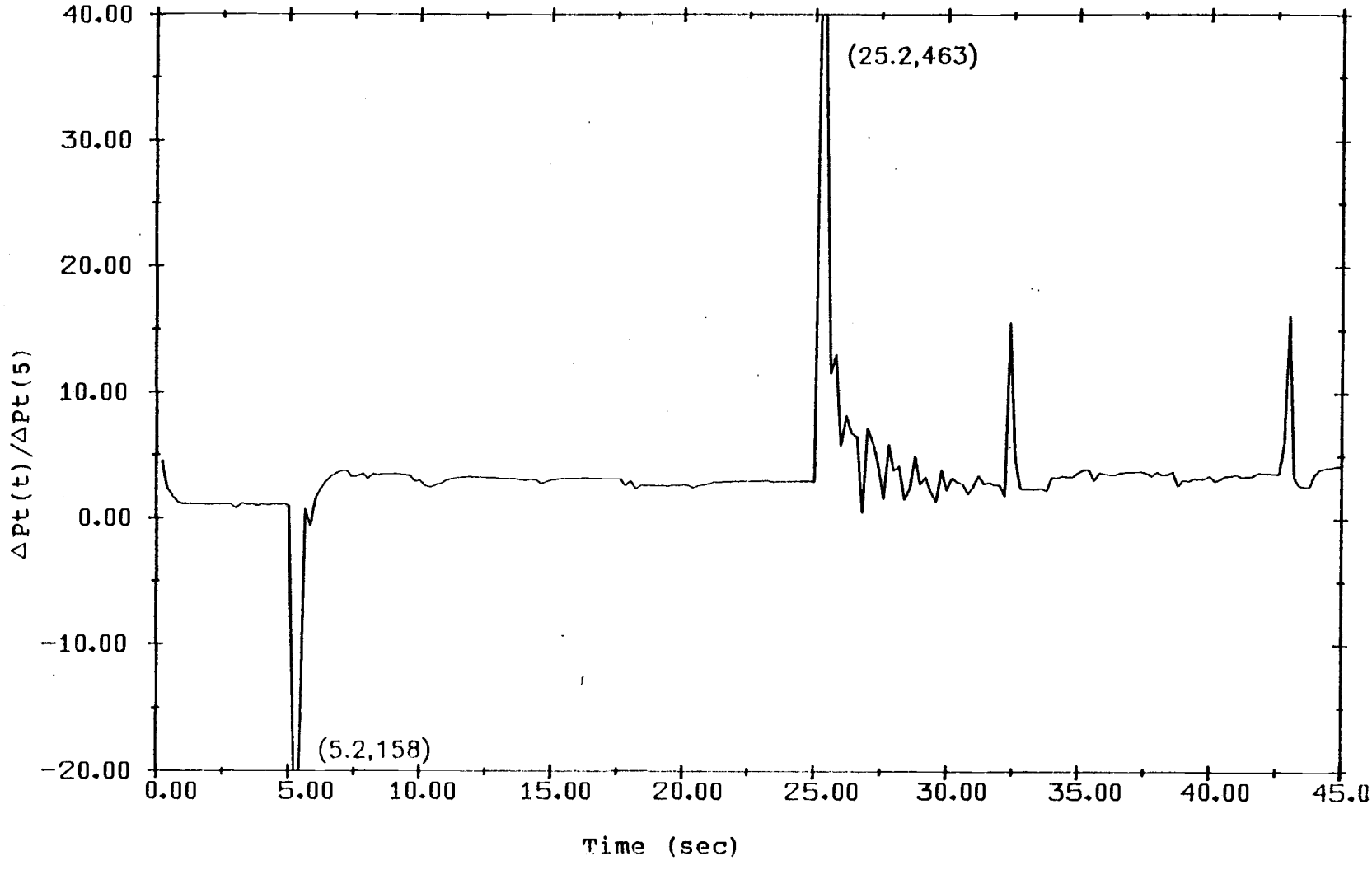

Figure 5-9 ΔPt(t)/ΔPt(5) for Case DT1

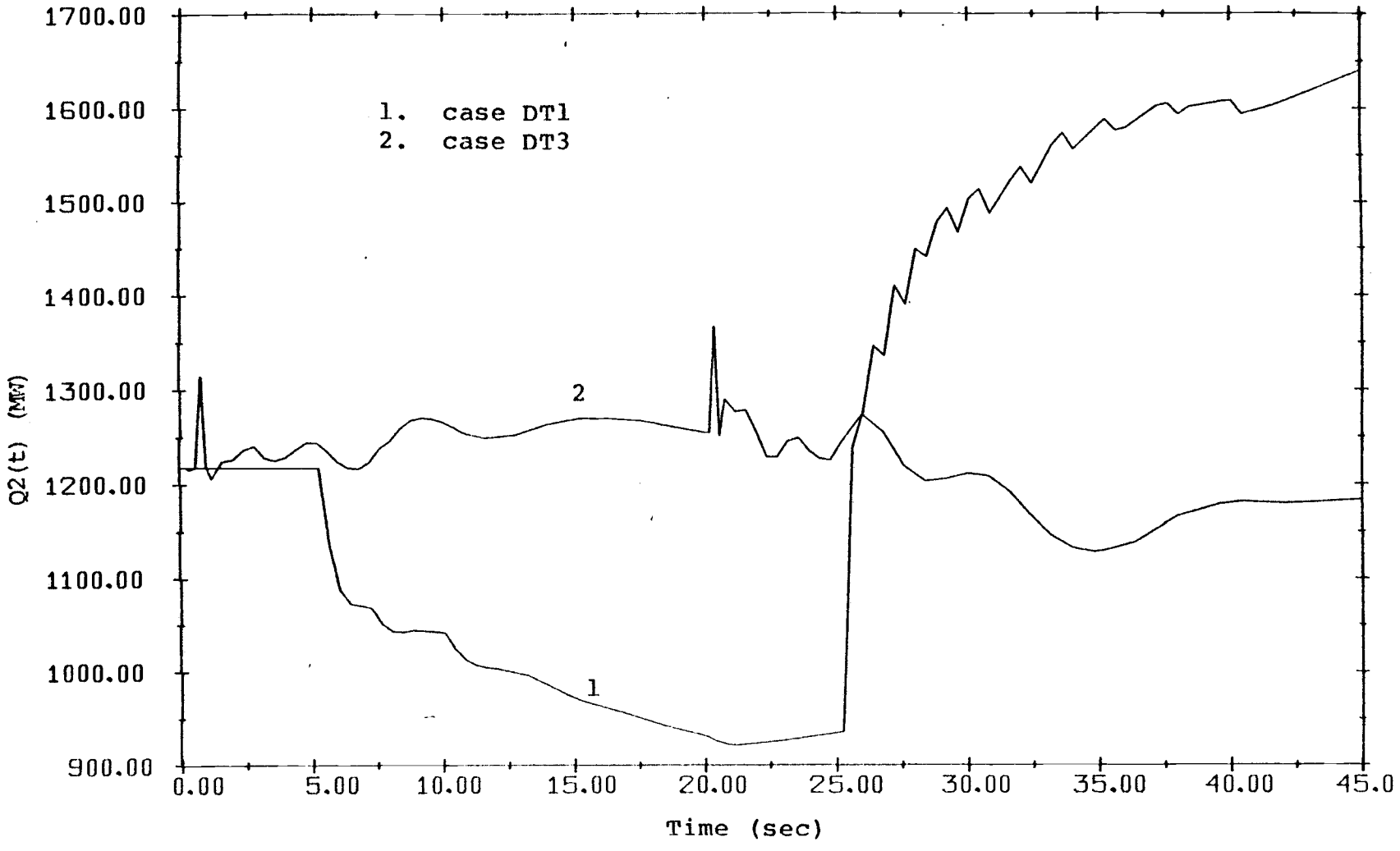

Figure 5-10 Heat Transfer into Secondary Side, Q2(t) for Case DT1 and DT3

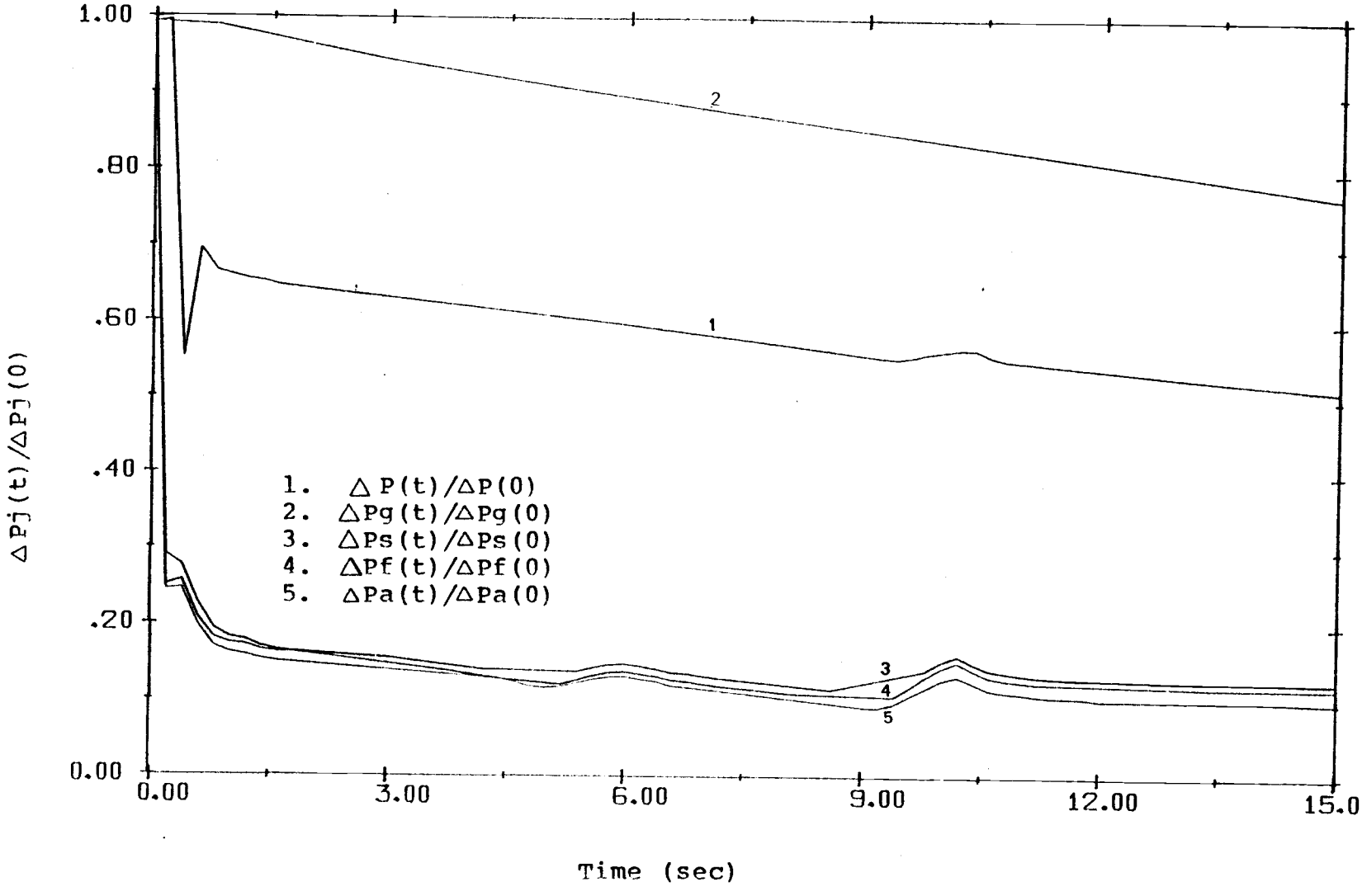

Figure 5-11 ΔPj(t)/ΔPj(0) for Case DT2

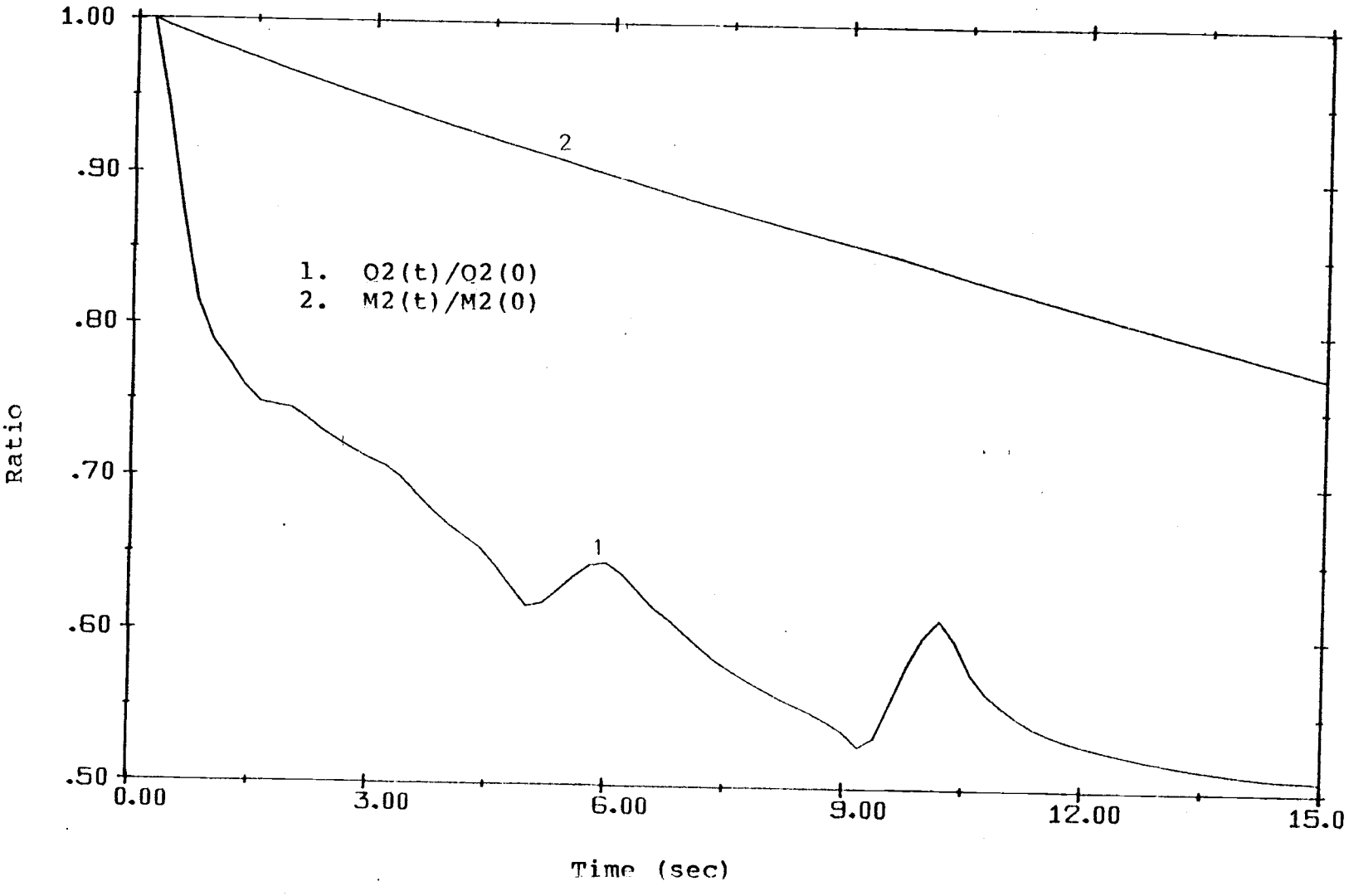

Figure 5-12 Relative Change of Q2 and M2 for Case DT2

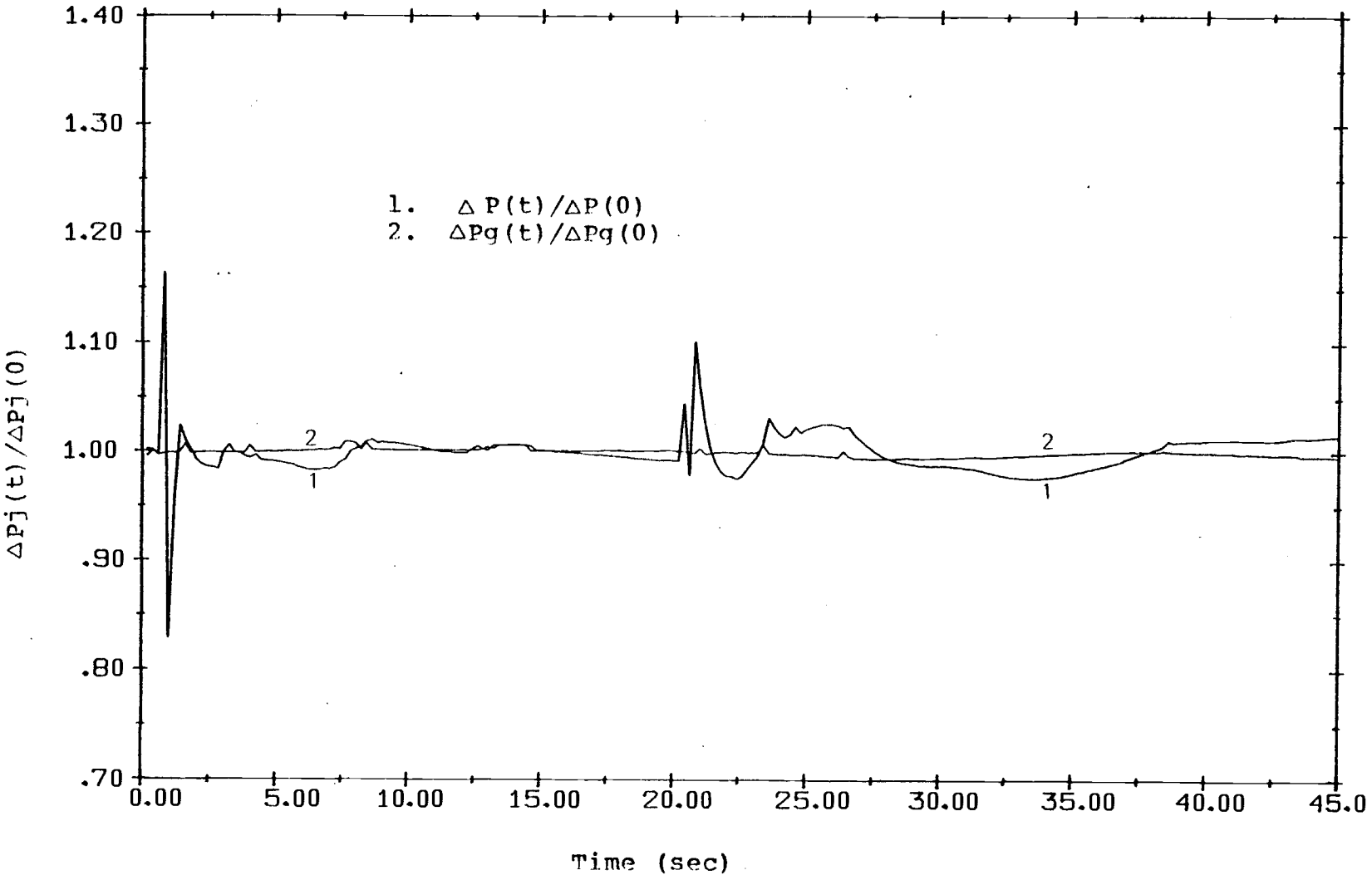

Figure 5-13 ΔPj(t)/ΔPj(0) for Case DT3

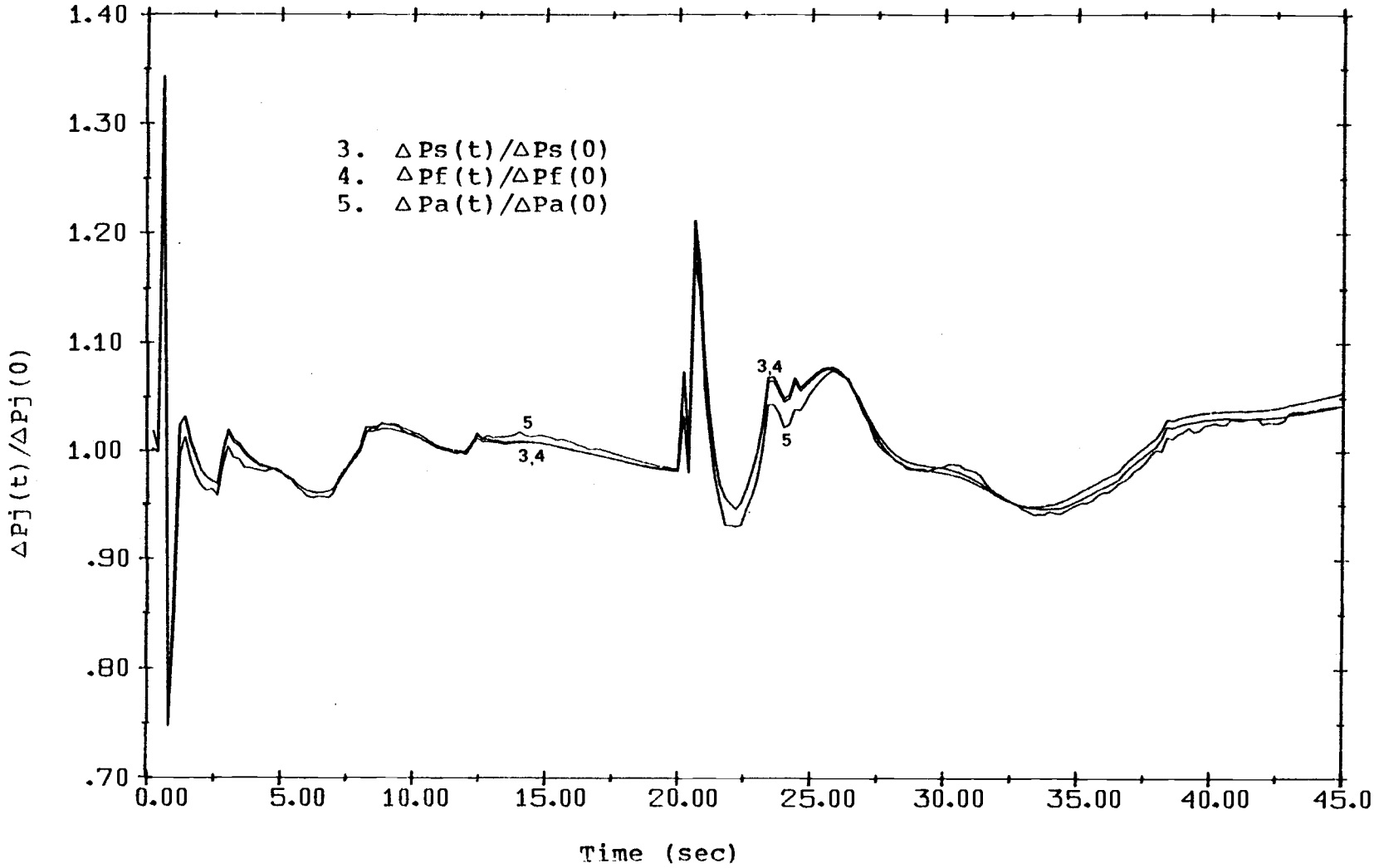

Figure 5-14 ΔPj(t)/ΔPj(0) for Case DT3

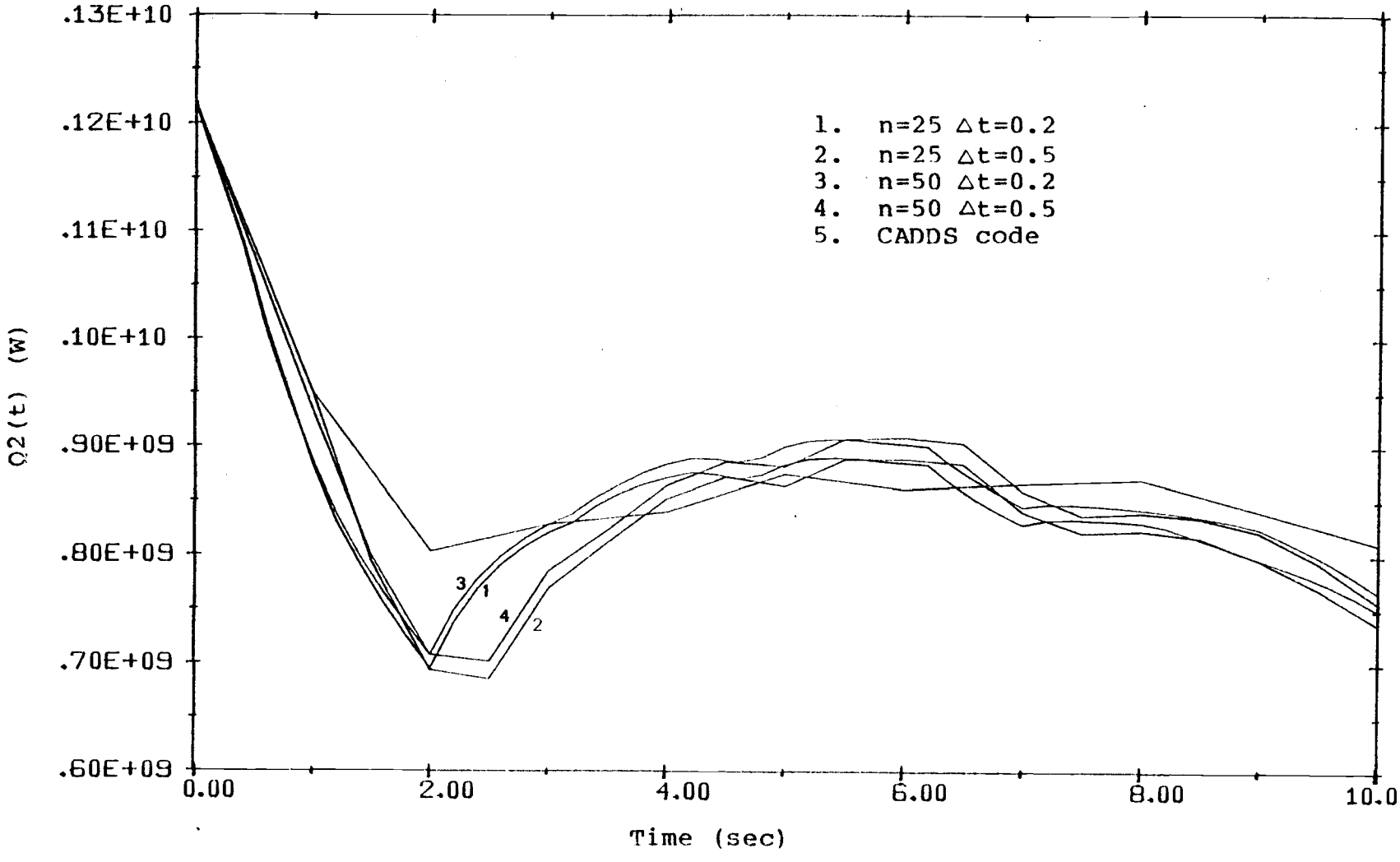

Figure 5-15 Heat Transfer into Secondary Side, Q2(t) for Case DT4

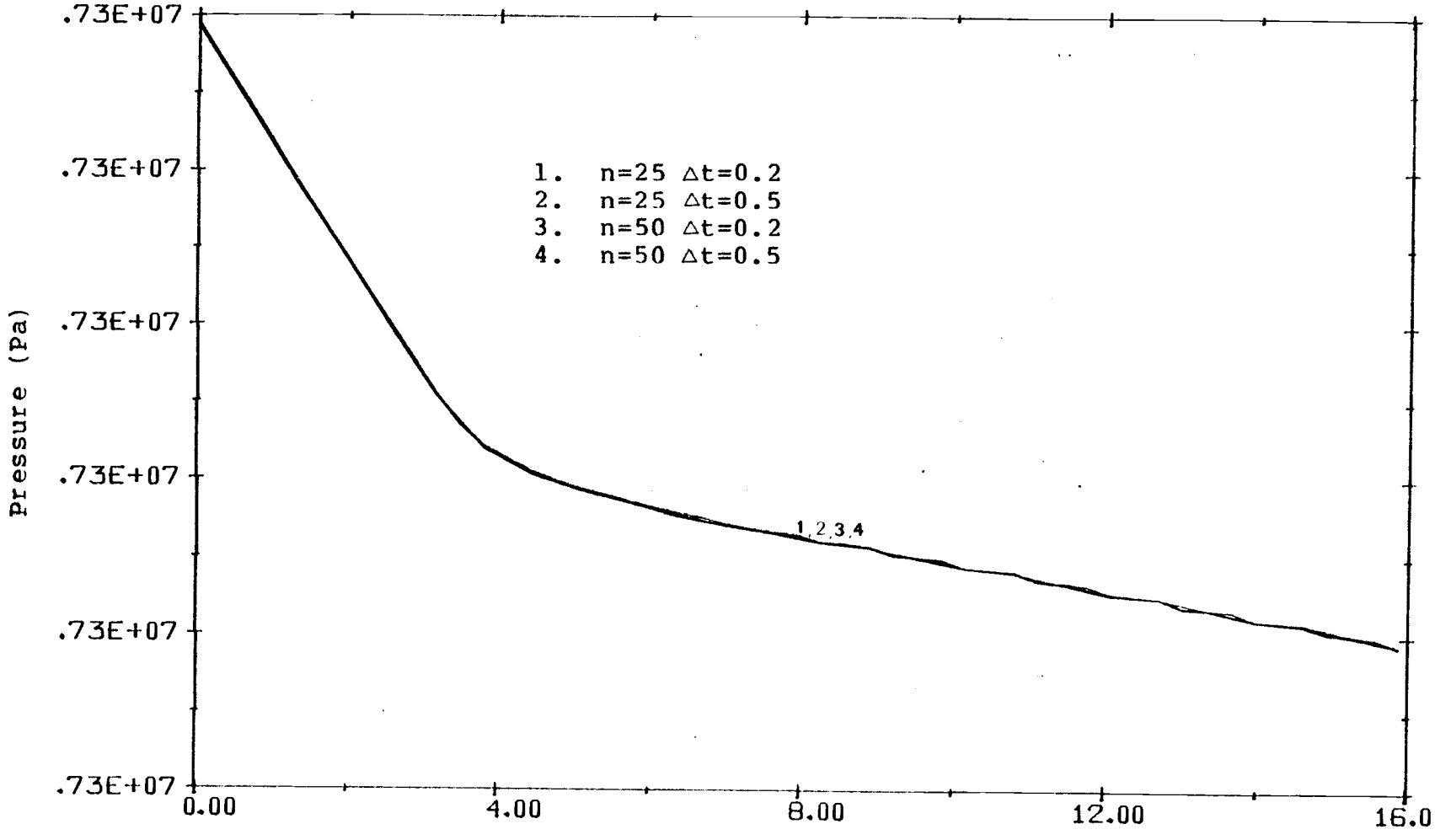

Figure 5-16 Pressure Profile for Case DT4

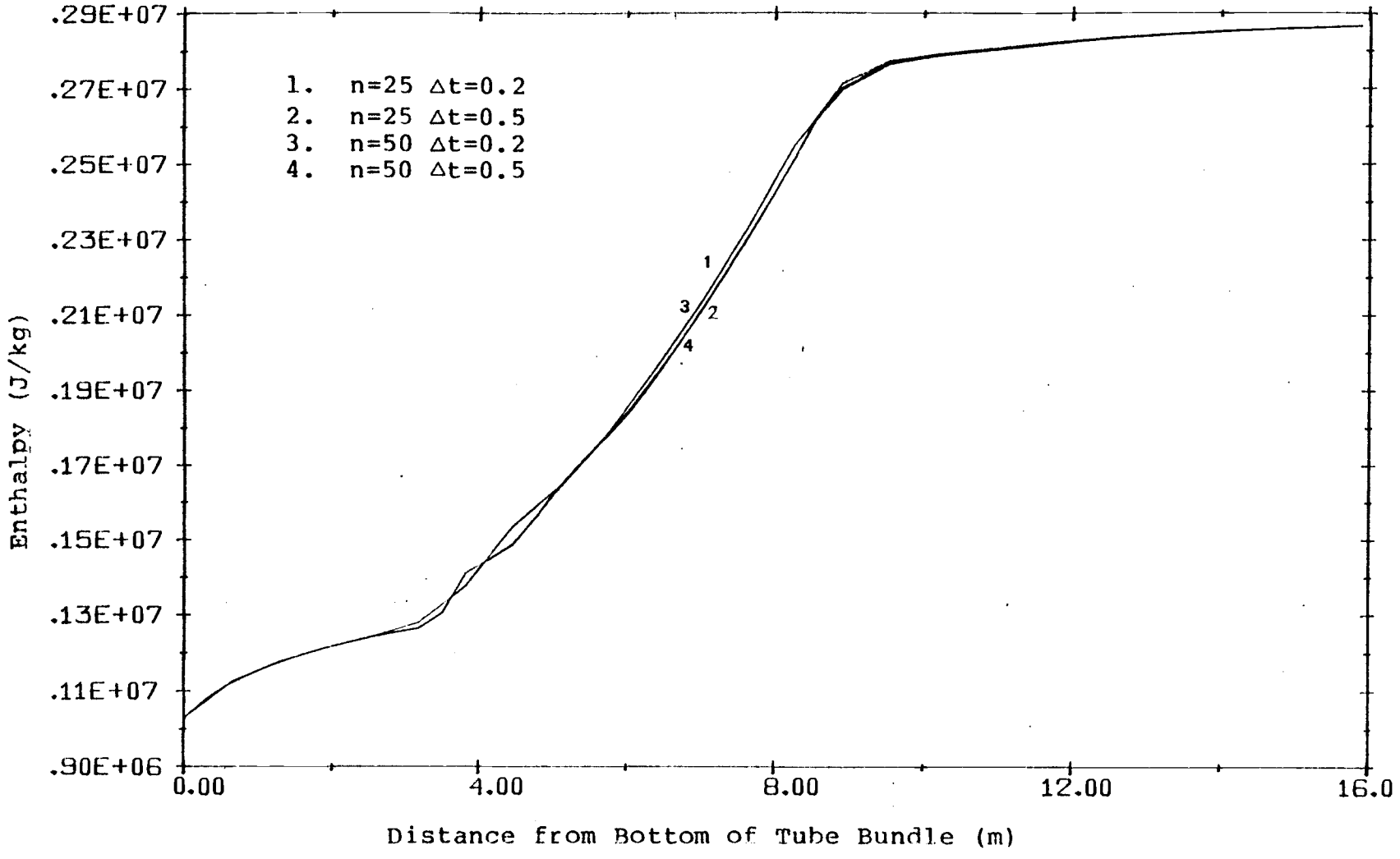

Figure 5-17 Enthalpy Profile for Case DT4

6. BIBLIOGRAPHY

1. B. N. McDonald and L. E, Johnson, "Nuclear Once-Through Steam Generator", A Paper Presented at American Nuclear Society Topical Meeting on Power Reactor Systems and Components, Williamsburg, Virginia (1970).

2. "Once-Through Steam Generator Research and development Report", BAW-10027, Babcock and Wilcox (1971).

3. "Davis-Besse Nuclear Power Station Unit No. 2 and 3, Final Safety Analysis Report", Toledo Edison (1974).

4. B. N. McDonald, R. C. Post and J. S. Scearce, "Once-Through Steam Generator Research and Development Report, Supp.1-Integral Economizer OTSG", BAW-10027, Supp.1, Babcock and Wilcox (1972).

5. "Babcock and Wilcox-205, Standard Safety Analysis Report (B-SAR-205)", Babcock and Wilcox (1976).

6. G. B. Wallis, One-Dimensional Two-Phase Flow, McGraw Hill Book Co., New York, (1969).

7. J. C. Lee et al., "Transient Modeling of Steam Generator Units in Nuclear Power Plants--a Critical Review", EPRI NP-1368 Project 684-1, (1980).

8. J. C. Lee et al., "Review of Transient Modeling of Steam Generator Units in Nuclear Power Plants", EPRI NP-1368 Project 684-1, (1980)

9. V. S. Arpaci, Conduction Heat Transfer, Addison-Wesley Publishing Co., Reading, Massachusetts, (1966).

10. B. Carnahm, et al., Applied Numerical Methods, J. Wiley and Sons (1969).

11. M. M. El-Wakil, Nuclear Heat Transport, International Textbook Co., New York, (1971).

12. W. M. Keys, Convection Heat and Mass Transfer, McGram-

Hill Book Co., New York., (1980).

13. L. S. Tong and J. Weisman, Thermal Analysis of Pressurized Water Reactor, ANS, (1970).

14. C. J. Baroczy, "A Systematic Correlation for Two-Phase Pressure Drop," NAA-SR-Memo-11858, (1966).

15. R. W. Lockhart and R. C. Martinell, "Proposed Correlation of Data for Isothermal Two-Phase, Two-Component Flow in Pipe." Chem. Eng. Prog., 45, 39 (1949).

16. R. W. Lockhart and D. B. Welson, "Prediction of Pressure Drops During Forced Circulation Boiling of Water." Trans. ASME, 70, 695 (1948).

17. K. V. Moore et al.,"Retran-A Program for One-Dimension Transient Thermal-Hydraulic Analysis of Complex Fluid Flow Systems", EPRI NP 408 Projects 342-1-1 & 889-2., (1977).

18. R. T. Fortino, "Thermal-Hydraulic Analysis of Once-Through Steam Generators." EPRI NP-1431 Project S137-1, (1980)

APPENDIX A. DESCRIPTION OF ONCE-THROUGH STEAM GENERATOR

This appendix presents a brief description of OTSG designs in PWR plants in order to provide fundamental definitions of the structural components, flow paths, heat transfer characteristics and operating parameters. Two types of steam generators, OTSG and IEOTSG, will be described in detail, and will be compared with each other.

A.1. OTSG

The Babcock and Wilcox (B&W) OTSG design produces superheated steam from subcooled feedwater and is used in all PWR plants built or licensed by B&W. This steam generator design as shown in Figure A-1, is a tube-and-shell, counter-flow heat exchanger. Reactor coolant flows downward through approximately 16000 tubes and transfers heat to the secondary coolant which flows upward along the shell side for generation of steam. The primary (reactor coolant) side of the steam generator includes the hemispherical inlet and outlet heads, tube sheets and inner tube surfaces. The secondary coolant is contained in the shell side of the steam generator, which is bounded by the shell, tube sheets and outer tube surfaces.

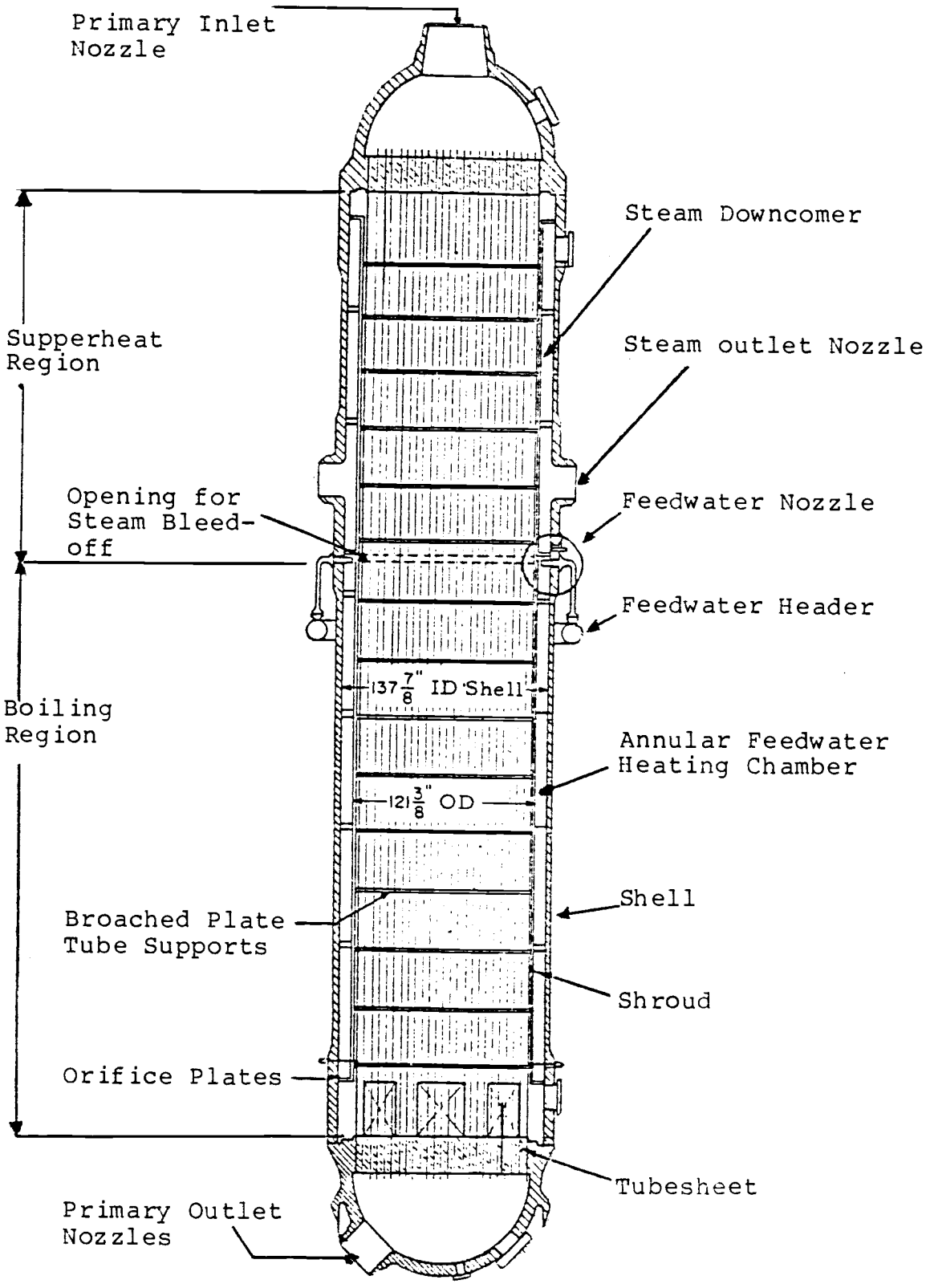

Figure A-1 Once-Through Steam Generator[1]

The tube bundle is surrounded by a cylindrical shroud which divides the secondary side into a feedwater heating chamber, an annular steam downcomer, and the heat exchanger region. Openings in the cylindrical baffle near the feedwater inlet nozzle level allow contact heating of feedwater in the feedwater heating chamber by bleeding off some of the steam from the tube bundle region. This is achieved by the inlet spray of feedwater which draws steam into the heating chamber by aspiration. After mixing, the feedwater nearly reaches saturation before entering the tube bundle region under normal operating conditions. The water level in the heating chamber is maintained so as to produce an elevation head which balances the pressure head of boiling water in the tube bundle and the pressure drop across the bypass flow openings.

The primary side heat transfer for the OTSG is subcooled by forced convection along the entire heat exchanger length during normal reactor operations. The secondary side of the heat exchanger may be divided into the following heat transfer regions:

A.1.1. Flow Boiling

The flow boiling region ranges from the lower tube sheet to the point where critical heat flux (CHF) conditions are reached. This normally occurs near the

openings for steam bleed-off. In the flow boiling region the quality of steam changes from near zero to near one. The major heat transfer mechanisms on the secondary side are nucleate boiling and forced convection vaporization. Boiling heat transfer is, in general, more efficient than the liquid or vapor single-phase forced convection process.

Nucleate boiling occurs when tube wall temperature and flow conditions allow a stable superheated fluid layer to form along the tube surface. Bubbles formed in the superheated layer detach and collapse in the saturated or subcooled bulk fluid, thus transferring the heat of bubble formation. Forced convection vaporization occurs at moderate to high steam quality, when an annular film flow pattern has developed. Heat transfer occurs by convection through the annular liquid flow and evaporation into the inner vapor core. For low flow rates, such as in natural convection, nucleate boiling is dominant in pre-CHF boiling heat transfer. For higher flow rates with moderate to high quality, the nucleate boiling process is disrupted and forced convection vaporization may become the dominant heat transfer mode. The secondary mass flow rate of the OTSG is low, but greater than that of the natural convection process. Thus, nucleate boiling and forced convection vaporization may coexist with significant contributions to heat transfer in the flow boiling region of an OTSG unit.

A.1.2. Film Boiling

Film boiling occurs after CHF has been surpassed. Since CHF occurs at high quality in the OTSG, the film boiling region is relatively short in length under normal conditions. In the film boiling heat transfer, the heat flux is sharply reduced during the transition from CHF to stable film boiling due to the formation of a vapor film along the tube surface. Heat transfer occurs by convection through the vapor film and evaporation of entrained liquid droplets in the saturated core.

A.1.3. Superheated Steam

When the quality of secondary steam reaches unity, the evaporation process ceases and superheating of the vapor begins. The heat transfer mechanism in superheating is single-phase forced convection.

The OTSG operates with constant primary coolant flow, constant average primary temperature and constant turbine throttle pressure over the normal load range from 15% to 100% load. The fact that the boiling heat transfer coefficient is much larger than the heat transfer coefficient of the superheating region makes the ratio of the length

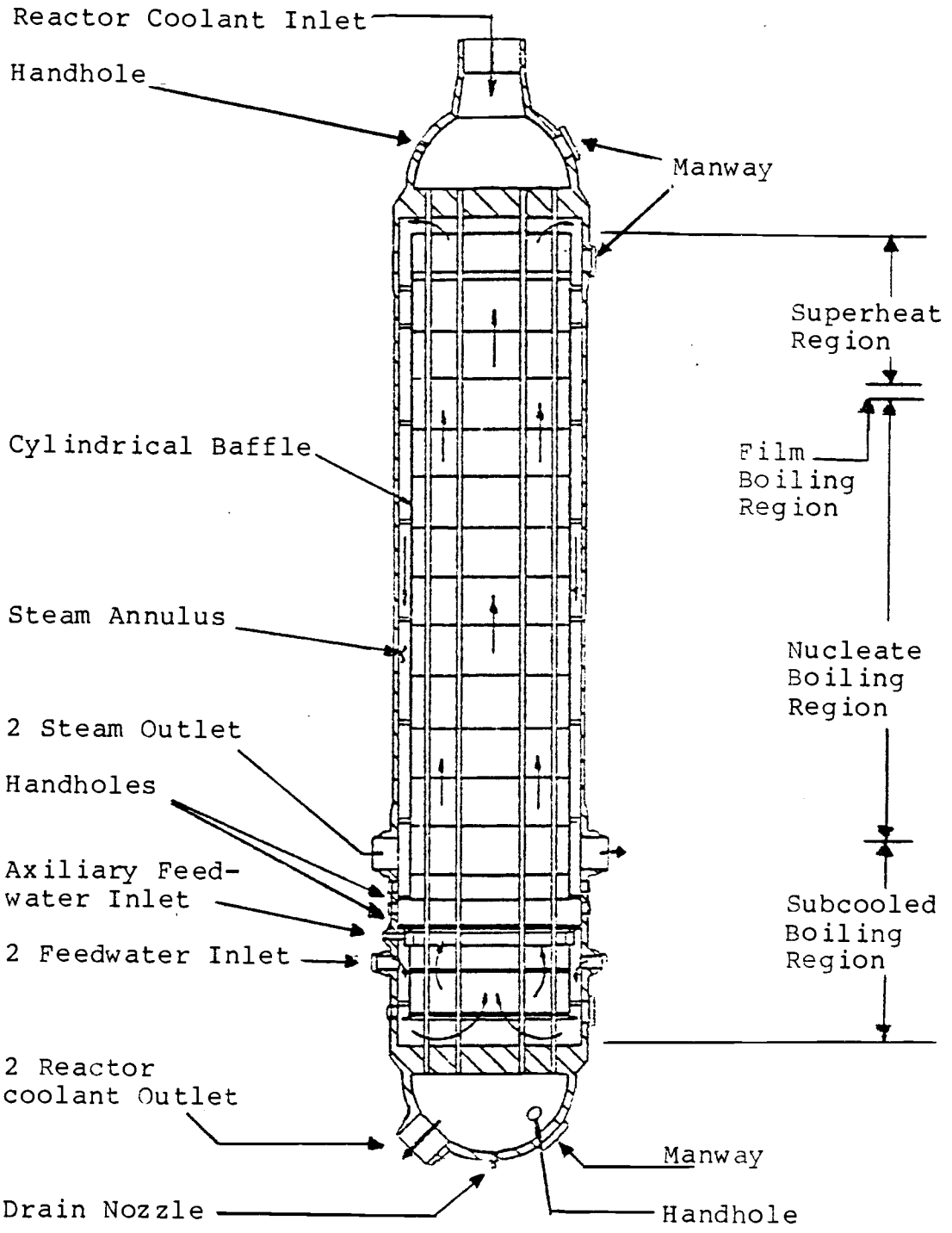

Figure A-2 IEOTSG[2]

Table A-1 Design Data for B&W Steam Generators[1-3]

Item	OTSG	IEOTSG
Steam conditions at full load, outlet nozzles		
Steam flow, kg/sec	741	1054
Steam temperature, C	308	308
Steam pressure, Pa	6.35E6	7.38E6
Feedwater temperature, C	235	240
Reactor coolant flow, kg/sec	8,290	10,010
Reactor coolant side		
Design pressure, Pa	1.73E6	1.73E6
Design/operating temperature, C		
Inlet	343/320	354/330
Outlet	354/291	354/298
Hydrotest pressure, Pa	2.16E7	2.16E7
Coolant volume (Hot), cu m	57.48	58.56
Secondary side		
Design pressure, Pa	7.32E6	8.59E6
Design temperature, C	315	332
Hydrotest pressure, Pa	9.12E6	1.07E7
Net volume, cu m	96.6	97.6
Dimensions		
Tubes, OD/min wall, cm	1.59/0.08636	1.59/0.08636
Overall height (including skirt), m	22.822	22.943
Shell OD or ID, m	3.743 (OD)	3.531 (ID)
Shell minimum thickness (at tube sheets & feedwater connect), m	0.12065	0.14605
Shell minmum thickness, m	0.0762	0.09525
Tube sheet thickness, m	0.549	0.549
Exposed tube length, m	15.88	15.88

the length of the boiling region to the superheating length on the secondary side one of the controlling parameters in load follow maneuvers. Other parameters are the primary coolant inlet temperature and feedwater flow rate. As plant load increases, these three parameters increase such that the OTSG outlet steam is able to generate enough power to meet the load demand. A decrease in the degree of superheating of the outlet steam will also simultaneously take place in such a maneuver due to a decrease in the superheating surface area.

A.2. IEOTSG

A more recent B&W OTSG design uses an integral economizer (IE) in the lower tube bundle region rather than feedwater heating by steam bleed-off. The NEW code has been developed specifically for this type of steam generator. A schematic diagram of the IEOTSG is shown in Figure A-2. Subcooled water flowing upward in the economizer region is heated to saturation very rapidly so that the superheating region begins at about the same elevation as in the OTSG design. There is no aspiration of feedwater by steam from the evaporation section. The characteristics of IEOTSG units with regard to load following maneuvers and heat transfer regions are otherwise very similar to those of OTSG units. A comparison of the design data for OTSG

and IEOTSG units is given in Table A-1.

REFERENCE

1. B. N. McDonald, R. C. Post and J. S. Scearce, "Once-Through Steam Generator Research and Development Report, Supp.1-Integral Economizer OTSG", BAW-10027, Supp.1, Babcock and Wilcox (1972).

2. "Babcock and Wilcox-205, Standard Safety Analysis Report (B-SAR-205)", Babcock and Wilcox (1976).

3. "Davis-Besse Nuclear Power Station Unit No. 2 and 3, Final Safety Analysis Report", Toledo Edison (1974).

APPENDIX B. THE GOVERNING EQUATIONS FOR ONE DIMENSIONAL CHANNEL FLOW

B.1. General Balance Equations

The governing equations for one-dimensional channel flow are obtained by appling a general property balance, i.e., equation B-1, to an infinitesimal control volume V, which is in the flow field. The cross section and wetted perimeter are denoted by S and Mw, respectively.

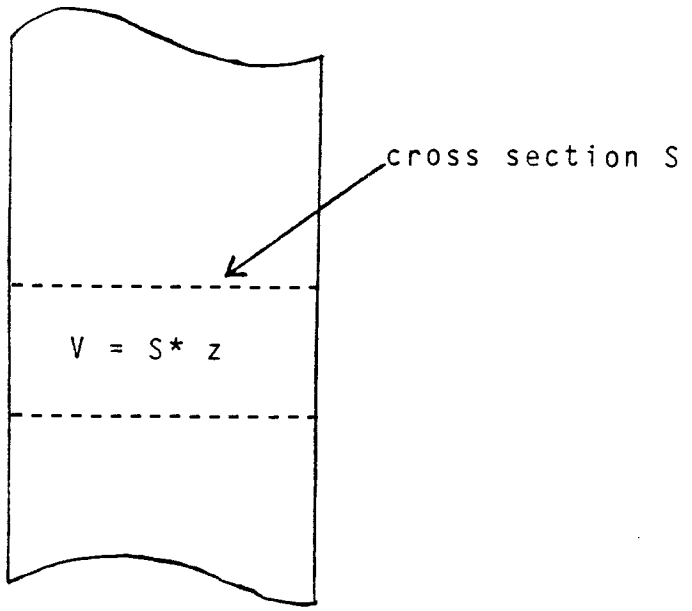

Figure B-1 Control Volume ΔV in Flow Field

They can be expressed as

$$S = (\pi/4) * Dh^{**}2$$

$$Mw = \pi * Dh$$

A representation of the flow field and the volume ΔV is shown in Figure B-1. The fluid stream velocity is denoted by v. The property per unit volume of material is denoted by W and stands for either the mass, or momentum, or energy per unit volume. The general balance statement for the property can be formulated as

$$\begin{bmatrix}\text{The time rate}\\ \text{of change of}\\ \text{W within } \Delta V\end{bmatrix} = \begin{bmatrix}\text{The net inflow}\\ \text{of W across the}\\ \text{surface of } \Delta V\end{bmatrix} + \begin{bmatrix}\text{Generation}\\ \text{of W}\\ \text{within } \Delta V\end{bmatrix} \qquad \text{(B-1)}$$

The time rate of change of W within ΔV is given by

$$\frac{\partial}{\partial t}(W * \Delta V) \qquad \text{(B-2)}$$

The net inflow of W is given by

$$S*[W(z)*v(z)-W(z+\Delta z)*v(z+\Delta z)]+Mw*\Delta z*Wc, \qquad \text{(B-3)}$$

where Wc is the radial inflow of property W across the wall per unit area per unit time. The generation of the

property within ΔV is given by

$$Wg*\Delta V \qquad (B-4)$$

where Wg is the generation (or loss) of the property per unit volume and unit time within the control volume. Substituting equation B-2, B-3 and B-4 into equation B-1 gives

$$\frac{\partial}{\partial t}(W*\Delta V) = S*[W(z)*v(z)-W(z+\Delta z)*v(z+\Delta z)]+ Wg*\Delta V+Mw*\Delta z*Wc.$$

Dividing above equation by ΔV gives

$$\frac{\partial}{\partial t}W = [W(z)*v(z)-W(z+\Delta z)*v(z+\Delta z)]/\Delta z+Wg+Mw*Wc/S \qquad (B-5)$$

The governing equations are obtained by substituting the property per unit volume, W; the radial inflow of property, Wc and the generation of the property, Wg into equation B-5. These governing equations are developed in the following section.

B.2. Continuity Equation

The conservation of mass, or the continuity equation,

is obtained as follows. The property W is the mass per unit volume, or the density ρ. The radial inflow of mass is zero. The generation of mass Wg is also zero. Equation B-5 becomes

$$\frac{\partial}{\partial t}\rho = - \frac{\partial}{\partial t}G, \qquad \text{(B-6)}$$

where $G=\rho*v$ is the mass flow rate per unit area.

B.3. Momentum Equation

The linear momentum balance, or momentum equation, is obtained as follows. The property W is the momentum per unit volume, i.e., $\rho*v=G$. The radial inflow of momentum is zero. The generation of momentum is the total force exerted on the control volume, or

$$\begin{aligned} Wg &= \Sigma F/\Delta V \\ &= \frac{[P(z)-P(z+\Delta z)]*S-\tau*Mw*\Delta z-g*\rho*\Delta V}{\Delta V} \\ &= - \frac{\partial}{\partial t}P- \tau*Mw/S-\rho*g, \end{aligned}$$

where P is the pressure, g is the gravitational constant, and τ is the shear stress per unit area between the wall and fluid. The shear force, τ is arbitrarily defined as

$$\tau = f * \frac{\rho v^2}{2}$$

where f is called friction factor as discussed in chapter 4. Equation B-5 becomes

$$\frac{\partial}{\partial t} G = - \frac{\partial}{\partial Z} (G^2/\rho) - \frac{\partial}{\partial Z} P - \tau * Mw/S - \rho * g \qquad (B-7)$$

or

$$\frac{\partial}{\partial t} G = - \frac{\partial}{\partial Z} P + R \qquad (B-8)$$

where

$$R = \left(\frac{\partial P}{\partial Z}\right)_{acc} + \left(\frac{\partial P}{\partial Z}\right)_{frict} + \left(\frac{\partial P}{\partial Z}\right)_{grav}$$

and

$$\left(\frac{\partial P}{\partial Z}\right)_{acc} = - \frac{\partial}{\partial Z} (G^2/\rho)$$

$$\left(\frac{\partial P}{\partial Z}\right)_{frict} = -\tau * Mw/S = - 2 * f * G^2 / (\rho * Dh)$$

$$\left(\frac{\partial P}{\partial Z}\right)_{grav} = -\rho * g$$

B.4. Energy Equation

Several forms of the energy equation can be written. Here the property W is taken as the internal energy per

unit volume,

$$W = \rho * u$$

where u is defined as the internal energy per unit mass. The radial inflow energy, Wc is q per unit area and time. The loss of energy Wg is the work done by volume change of the fluid,

$$Wg = - \frac{Work}{\Delta V}$$

$$= - \frac{[P(z+\Delta z)*v(z+\Delta z)-P(z)*v(z)]*S}{\Delta V}$$

Let Δz be infinitestimally small; we get

$$Wg = - \frac{\partial}{\partial z}(P*v)$$

Therefore, equation B-5 becomes

$$\frac{\partial}{\partial t}(\rho*u) = - \frac{\partial}{\partial z}(\rho*v*u)+Mw*q/S- \frac{\partial}{\partial z}(P*v),$$

or

$$\frac{\partial}{\partial t}(\rho*h) = - \frac{\partial}{\partial z}(G*h)+4*q/Dh+\frac{\partial}{\partial z}P \qquad (B-9)$$

where h is the enthalpy which is defined as

$$h = u+P/\rho.$$

APPENDIX C. NEWTON'S METHOD FOR ROOT FINDING

We define the secondary exit pressure as a function of the inlet pressure

$$P2o = f(P2i) \tag{C-1}$$

Let the prescribed boundary condition P2o be PE. Our purpose is to find an inlet pressure PI which satisfies

$$PE = f(PI) \tag{C-2}$$

as shown in Figure C-1.

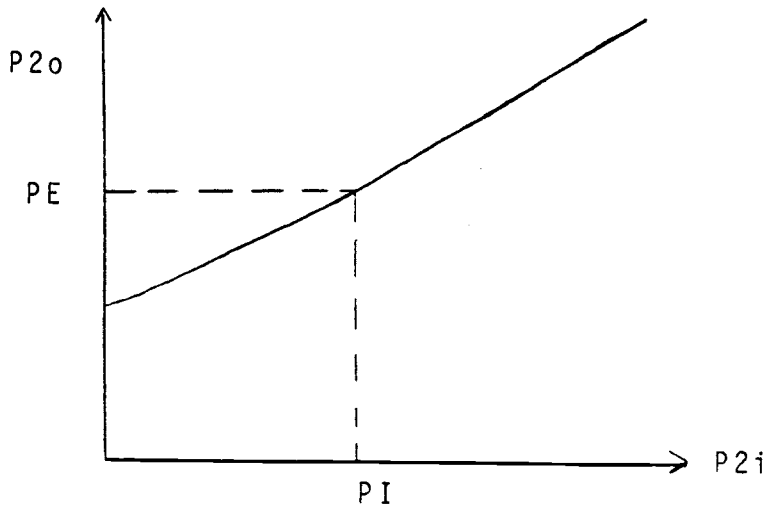

Figure C-1 The Relation between P2o and P2i

Define a function as

$$F(Pi) = PE - f(Pi) \tag{C-3}$$

Then the root PI of F(Pi) satisfies equation C-1. Appling Newton's method to equation C-3, we get

$$Pi^{(n+1)} = Pi^{(n)} - F(Pi^{(n)})/F'(Pi^{(n)})$$

or

$$Pi^{(n+1)} = Pi^{(n)} + [PE - f(Pi^{(n)})]/f'(Pi^{(n)}) \tag{C-4}$$

We use the first order polynomial approximation for $f'(Pi^{(n)})$, and get

$$f'(Pi^{(n)}) = [f(Pi^{(n)}) - f(Pi^{(n-1)})]/(Pi - Pi^{(n-1)})$$

or

$$f'(Pi^{(n)}) = (Po^{(n)} - Po^{(n-1)})/(Pi^{(n)} - Pi^{(n-1)}) \tag{C-5}$$

Substituting equation C-5 into equation C-4, we get

$$Pi^{(n+1)} = Pi^{(n)} + (PE - Po^{(n)})(Pi^{(n)} - Pi^{(n-1)})/(Po^{(n)} - Po^{(n-1)}) \tag{C-6}$$

APPENDIX D. ITERATION SCHEME FOR SOLVING THE SYSTEM OF DESCRIBING EQUATIONS

The flow chart for integrating the steady state and transient equations are shown in Figure D-1 and Figure D-2, respectively. In steady state, the time derivatives of the conservation equations are zero. Thus the basic equations become

$$G = \text{constant} \tag{D-1}$$

$$-\frac{\partial P}{\partial z} + R = 0 \tag{D-2}$$

$$-\frac{\partial}{\partial z}(G*h) + 4*qw/Dh = 0 \tag{D-3}$$

$$\rho = \rho(P,h) \tag{D-4}$$

$$Tb = Tb(P,h) \tag{D-5}$$

$$qw = H*(Tb-Ts). \tag{D-6}$$

Furthermore the equation for conduction of heat through the tube walls, which couple the primary and secondary side becomes

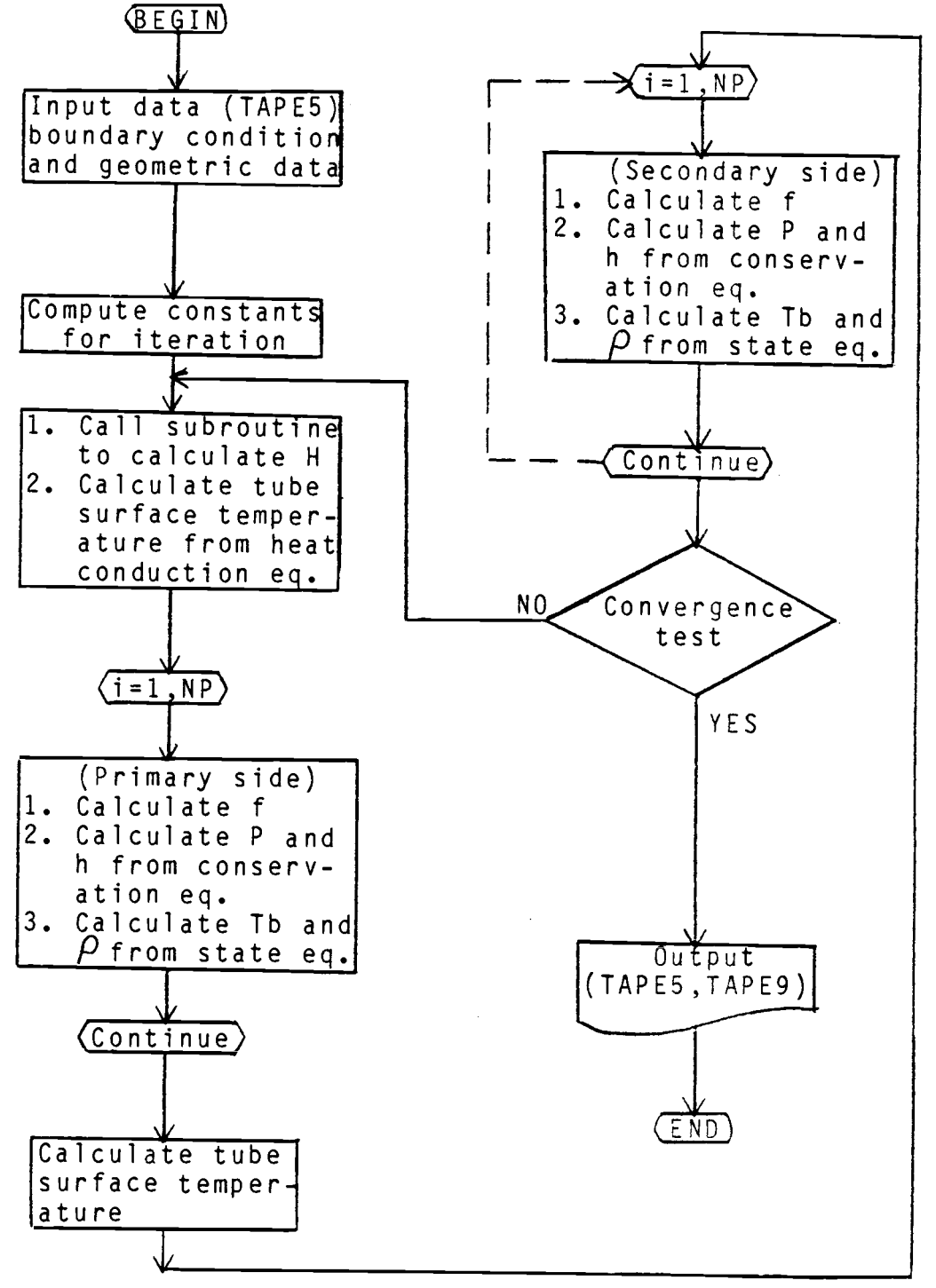

Figure D-1 Flow Chart for Steady State Calculation

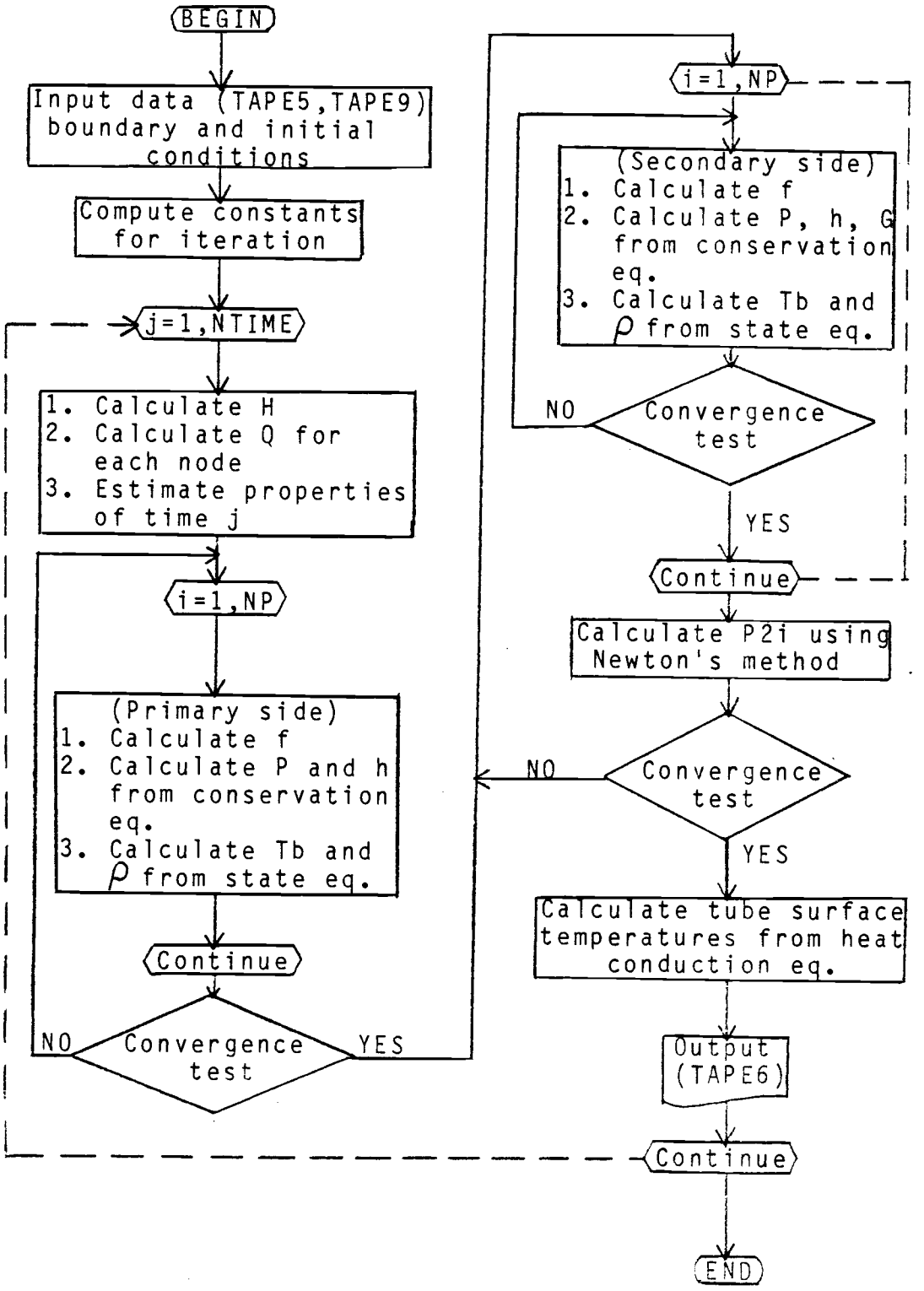

Figure D-2 Flow Chart for Transient Calculation

becomes

$$\frac{1}{r}\left[\frac{\partial}{\partial r}\left(Kt*r*\frac{\partial Tt}{\partial r}\right)\right] = 0 \qquad (D\text{-}7)$$

These simultaneous equations are solved numerically.

As shown in Figure D-1, the input data (i.e., TAPE5) contain the boundary condition and geometric information. The next step is to compute those parameters which remain constant during the iteration and to provide guessed values for the unknown properties to start the iteration. The iteration is based on successive replacement. The iteration scheme of the NEW code can be divided into four steps:

(1) calculate Tt from heat conduction equation.

(2) calculate P1, h1, T1, ρ1 and qw1 from conservation equations, state equations and Newton's equation of heat conduction.

(3) same as (1).

(4) same as (2) for secondary side.

After this procedure, we check for convergence of h and P in each node. If satisfied, we exit from the iteration loop; if not, we start over from the first step. The convergence criterion is defined as

$$ABS[(W^{(n+1)}(I)-W^{(n)}(I))*NP/(Wi-Wo)].LE.EPS$$

where W(I) is the property at node I, superscript (n) represents the number of the iteration, subscript i and o represent inlet and outlet condition, NP is the number of spatial mesh points and EPS is a given convergence parameter. In the program a limit is set on the maximum number of iterations in order to avoid excessive use of computer time under divergent conditions. If the iteration procedure has not converged within the maximum number of iterations, the NEW code stops and prints out an error message. If it converges the output will contain two files; one is written under the name TAPE6 and is intended for printing; the other is a file named TAPE9 which is used as input for the subsequent transient calculation (geometric information and initial condition).

In the transient calculation, we introduce a new scheme to solve the simultaneous equations. Examining equation 2-1 through 2-5, we find that there are five equations for six unknowns. The particular unknown qw is the only link between primary and secondary side. For any given qw we can solve these five equations for five unknowns (i.e., P, h, Tb, ρ, G) without considering the coupling condition. If we use the heat flux from the previous time step (explicit formulation), then the 13 simultaneous equations become three independent simultaneous sets, five equations for the primary side,

five for the secondary side and three for the tube wall.

By this scheme we have uncoupled the radial heat conduction solution from the solution of the fluid flow equations for primary and secondary fluid. Moreover, this scheme avoids convergence difficulty resulting from the discontinuity of the heat transfer coefficient as evaluated from correlations for different heat transfer regimes. From an economic point of view, this scheme enables us to independently solve the time-dependent fluid flow equations for the primary and the secondary side of the steam generator; this means a considerable reduction in computing effort. The justification for this scheme lies in the fact that the heat conduction transients occur on a slower time scale than fluid flow transients (i.e., convection transients), and we expect this scheme to be convergent over a wide range of conditions.

The flow chart for the transient calculation is shown in Figure D-2. First we input the boundary conditions, initial conditions and geometric information from TAPE5 and TAPE9 (i.e., output of steady state). Then we prepare parameters which remain constant during the iteration process and start the first time step. For each time step, we solve the three sets of equations as follows:

(1) solve for P1, G1, T1, ρ1 and h1 for primary side.

(2) same as (1) for secondary side